CHAMP1 complex directs heterochromatin assembly and promotes homology-directed DNA repair

Feng Li[1,*], Tianpeng Zhang[3], Aleem Syed[1], Amira Elbakry[1], Noella Holmer[1], Huy Nguyen[1,2], Sirisha Mukkavalli[1], Roger A. Greenberg[3], Alan D. D'Andrea[1,2,4,*]

1 Division of Radiation and Genome Stability, Department of Radiation Oncology, Dana-Farber Cancer Institute, Harvard Medical School, Boston, MA 02215, USA.

2 Center for DNA Damage and Repair, Dana-Farber Cancer Institute, Harvard Medical School, Boston, MA 02215, USA.

3 Department of Cancer Biology, Penn Center for Genome Integrity, Basser Center for BRCA, Perelman School of Medicine, University of Pennsylvania, Philadelphia, PA, USA

4 Lead contact

*Corresponding authors: feng_li@dfci.harvard.edu, alan_dandrea@dfci.harvard.edu

KEY WORDS: CHAMP1, SETDB1, H3K9me3, Telomere, Homologous recombination

ABSTRACT

The CHAMP1 complex, a little-known but highly conserved protein complex consisting of CHAMP1, POGZ, and HP1α, is enriched in heterochromatin though its cellular function in these regions of the genome remain unknown. Here we show that the CHAMP complex promotes heterochromatin assembly at multiple chromosomal sites, including centromeres and telomeres, and promotes homology-directed repair (HDR) of DNA double strand breaks (DSBs) in these regions. The CHAMP1 complex is also required for heterochromatin assembly and DSB repair in highly-specialized chromosomal regions, such as the highly-compacted telomeres of ALT (Alternative Lengthening of Telomeres) positive tumor cells. Moreover, the CHAMP1 complex binds and recruits the writer methyltransferase SETDB1 to heterochromatin regions of the genome and is required for efficient DSB repair at these sites. Importantly, peripheral blood lymphocytes from individuals with CHAMP1 syndrome, an inherited neurologic disorder resulting from heterozygous mutations in *CHAMP1*, also exhibit defective heterochromatin clustering and defective repair of local DSBs, suggesting that a defect in DNA repair underlies this syndrome. Taken together, the CHAMP1 complex has a novel role in heterochromatin assembly and the enhancement of HDR in heterochromatin.

INTRODUCTION

DNA double strand breaks (DSBs), resulting from intrinsic DNA replication errors or from external exposure to DNA damaging agents, can occur at any site throughout the genome. Homology-directed repair (HDR), including classical homologous recombination (HR) and break-induced replication (BIR), functions to repair these DSBs. Some regions of chromosomes may require specific mechanisms of DSB repair. For example, heterochromatic regions of chromosomes, such as centromeres and telomeres, are highly-compacted structures and pose a significant barrier to HDR-mediated DSB repair. Accordingly, cells may require distinct mechanisms to mediate HDR in these chromosomal regions[1-4].

Heterochromatin regions of the genome are characterized by increased trimethylation of histone H3 on lysine 9 (H3K9me3), a key modification that interacts with histone reader proteins[5] and is critical for heterochromatin clustering and function[6]. Heterochromatin assembly is regulated by the coordinated activity of writer H3K9 methyltransferases and eraser H3K9 demethylases. These enzymes regulate the level of H3K9me3 in heterochromatin[6,7], and these mechanisms are coupled to the HDR repair process[8-12].

Some heterochromatin structures have a unique nucleosome organization, and these structures may also require specialized mechanisms for heterochromatin assembly and local HDR repair. For example, approximately 10-15% of cancers employ a telomerase-independent mechanism known as the alternative lengthening of telomeres (ALT pathway). This process relies on HDR for template driven telomere lengthening by a break induced replication-like mechanism[13,14]. Moreover, ALT tumor cells have a high level of H3K9me3 and a specialized heterochromatic microenvironment that facilitates DNA synthesis and telomere expansion[15,16]. Whether the CHAMP1 complex plays a specific role in ALT telomere maintenance or ALT telomere DSB repair remains unknown.

A previous report[17] identified a distinct heterochromatin complex- namely, the CHAMP1/POGZ/HP1α complex- with H3K9me3-binding activity. CHAMP1 (CHromosome Alignment Maintaining Phosphoprotein 1), a highly-conserved zinc finger protein, functions as a regulator of chromosome segregation in mitosis and is required for correct alignment of chromosomes on the metaphase plate[18]. The CHAMP1 binding partner POGZ (POGO transposable element with ZNF domain), also a zinc-finger protein, functions in mitotic cell cycle progression and kinetochore assembly[19]. HP1α, a member of the HP1 family of "hub

proteins", interacts with several chromosomal proteins and binds to H3K9me3 through its chromodomain (CD). Whether this CHAMP1/POGZ/HP1α complex regulates heterochromatin assembly or mediates HDR in condensed regions of chromosomes remains unknown.

Humans with *de novo* heterozygous mutations in *CHAMP1*, known as CHAMP1 syndrome, present with a neurodevelopmental disorder characterized by intellectual disability, behavioral symptoms, and distinct dysmorphic features [20-24]. Interestingly, *de novo* heterozygous mutations in the *POGZ* gene also result in a rare but highly-related neurodevelopment syndrome called the White Sutton Syndrome (WSS) [25-33]. Whether these inherited mutations result from defects in heterochromatin assembly or HDR in heterochromatin remains unknown.

Recent studies have elucidated at least one mechanism by which CHAMP1 and POGZ promote HR [34-36]. CHAMP1 has a unique, high affinity site for the DNA repair HORMA protein, REV7. By binding to REV7, the CHAMP1/POGZ complex steals REV7 from the Shieldin (REV7/SHLD) complex[36]. The Shieldin complex normally blocks DNA end resection, promotes NHEJ repair, and inhibits HR repair [37-41]. By binding to REV7, the CHAMP1/POGZ complex increases DSB end resection and promotes HR repair. Whether this mechanism of enhanced HR repair occurs in heterochromatin, or whether its use is confined to euchromatic regions, remains unknown.

In the current study we show that the CHAMP1/POGZ/HP1α heterochromatin complex performs a direct role in heterochromatin clustering and HDR repair. The complex promotes the deposition of H3K9me3, the clustering of heterochromatin, and the recruitment of HDR proteins (both HR proteins and BIR proteins) to DSBs at heterochromatic sites. While the complex subunits promote heterochromatin clustering at multiple sites, including centromeres and telomeres, it has a distinct and obligate role in maintaining ALT telomeres. Depletion of the CHAMP1/POGZ/HP1α complex results in reduced H3K9me3 and loss of heterochromatin clustering. Interestingly, the POGZ subunit also binds and recruits the methyltransferase SETDB1 to sites of heterochromatin. Finally, peripheral blood lymphocytes from individuals with CHAMP1 syndrome also exhibit defective heterochromatin clustering and HR, suggesting that a defect in DNA repair underlies this syndrome. Taken together, the CHAMP1/POGZ/HP1α is a novel molecular machine which regulates heterochromatin clustering and contributes to local HDR repair in heterochromatin.

RESULTS

Structural modelling of the heterochromatic CHAMP1-POGZ-HP1α complex

Quantitative proteomic analyses of histone epigenetic marks and readers identified CHAMP1-POGZ-HP1α as a heterochromatin complex that binds H3K9me3[17]. Recent studies have shown that the CHAMP1[34,36] and POGZ subunits[35] promote HR-mediated DSB repair through interaction with REV7. Nevertheless, the relationship between the heterochromatin localization of the complex and HR is unclear.

To investigate the organization of the multi-subunit CHAMP1 complex, we performed *in silico* structural modeling of binary interactions among the subunits with AlphaFold2-Multimer (AF2)[42,43]. This allowed us to predict a high-confidence interaction between the CHAMP1 N-terminal ZnF domain (1-87 aa) and the structured C-terminus of POGZ (1021-1410 aa) (**Fig. 1a,b**). The interaction between CHAMP1 and POGZ is formed primarily by hydrophobic residues at the interface (**Fig. 1a**). Conversely, our modelling showed that the CHAMP1 C-terminal ZNF domain forms an extended β-sheet-type interaction with residues (16-22 aa) from the N-terminus of HP1α (**Extended Data Fig. 1a**). Furthermore, HP1α homodimerizes through its C-terminal chromodomains (**Extended Data Fig. 1b**), while the HPZ domain of POGZ interacts with the same C-terminal chromodomain of HP1α from the opposite side of the dimerization interface (**Extended Data Fig. 1c**). Since CHAMP1 binds to the same site on the N-terminus of HP1α as H3K9me3, HP1α homodimerization through its C-terminal chromodomain may allow a HP1α dimer to bind CHAMP1 and H3K9me3 simultaneously.

Through these AF2 predictions and previously published studies on the interactions between POGZ and HP1α[19], HP1α and H3K9me3 [5], and HP1α dimerization [44,45], we built a composite structural model of the CHAMP1 complex containing CHAMP1, POGZ, HP1α and H3K9me3 (**Fig. 1c**). In this model, the N-terminus of CHAMP1 interacts with POGZ, while the C-terminus of CHAMP1 directly engages with an HP1α dimer[5]. The CHAMP1-POGZ-HP1α complex appears to function as a bridge, connecting two H3K9me3. We next validated these predictions using a series of mutations in CHAMP1 and HP1α (homodimerization mutant) (**Fig. 1c-f, and Extended Data Fig. 1d**). As expected, N-terminal mutants of CHAMP1 (ΔN, ΔNΔC and QLT/RRR) failed to bind to POGZ (**Fig. 1d, lanes 7,8, and Extended Data Fig. 1d, lane 6**), and C-terminal mutants of CHAMP1 (ΔNΔC and ΔC) failed to bind to HP1α (**Fig. 1d, lane 8,**

and Fig. 1e, lane 10). Furthermore, the HP1α dimerization mutant I165E[19,44] failed to bind to CHAMP1, while POGZ could independently bind to HP1α and H3K9me3 (**Fig. 1f, lane 6**).

Interestingly, the GFP-CHAMP1-2A mutant, which failed to bind to REV7, still pulled down POGZ and HP1α (**Fig. 1e, lane 8**), suggesting that REV7 is not required for the formation of the CHAMP1/POGZ/HP1α heterochromatin complex. GFP-HP1α successfully pulled down CHAMP1, POGZ, and H3K9me3, but did not pull down REV7 (**Fig. 1g, lanes 5,6**). Moreover, GFP-REV7 pulled down CHAMP1 and POGZ but did not pull down HP1α or H3K9me3 (**Fig. 1h, lanes 5,6**). Taken together, our data suggest that the CHAMP1 complex may function in a REV7-independent pathway while interacting with heterochromatin.

CHAMP1 complex promotes heterochromatin clustering at multiple genomic regions

To investigate the potential function of the CHAMP1 complex in the formation of heterochromatin clusters, we initially assessed the localization of CHAMP1 and POGZ within heterochromatin foci by immunofluorescence. Remarkably, we observed a strong colocalization of CHAMP1 and POGZ with H3K9me3, which we used as a marker of heterochromatin, in human U2OS and mouse NIH-3T3 cells. Colocalization was further enhanced by ionizing radiation (IR) induced DSBs (**Fig. 2a,b and Extended Data Fig. 2a,b**). Consistently, the association between CHAMP1 and HP1α was stronger after cellular exposure to IR (**Extended Data Fig. 2c**). This interaction was not affected by the loss of REV7 interaction (i.e., the CHAMP1-2A mutant), supporting the idea that the CHAMP1 heterochromatin complex functions independently of REV7. Interestingly, radiation also induced the interaction of H3K9me3 with HP1α, but not with HP1β or HP1γ (**Extended Data Fig. 2d**), suggesting a specific role of HP1α in the heterochromatin enrichment at DSBs.

Notably, the CRISPR-knockout (KO) of CHAMP1 or POGZ in U2OS cells resulted in a significant reduction in the formation of H3K9me3 and HP1α foci (**Fig. 2c-f**). However, the knockout of CHAMP1 or POGZ did not affect the overall expression level or chromatin binding of H3K9me3 and HP1α (**Extended Data Fig. 2e,f, lane 9-12**). To further determine whether the CHAMP1 heterochromatin complex promotes H3K9me3 accumulation at centromeres and telomeres, well-known heterochromatin sites, we next performed immunofluorescence with a centromere marker (Cent FISH) or a telomere marker (anti-TRF2 antibody)[46]. As expected, we observed a significant loss of H3K9me3 foci at both centromeres and telomeres following

deletion of the CHAMP1 or POGZ in U2OS cells (**Fig. 2g-j).** Consistently, ChIP-qPCR also demonstrated a decreased level of H3K9me3 at telomeres in CHAMP1 or POGZ KO U2OS cells (**Fig. 2k**). Taken together, the CHAMP1 complex plays a role in assembling the H3K9me3 heterochromatin mark at multiple sites in the genome, including sites with damage-induced DSBs as well as at centromeres and telomeres.

Recent studies on telomeres in ALT tumor cells suggest a distinctive heterochromatin structure characterized by high levels of H3K9me3, low levels of ATRX, and elevated HDR processes at telomeres[47-49]. We therefore decided to investigate the possible role of the CHAMP1 complex in the maintenance of these ALT telomere structures and HDR repair. We first examined the possible localization of the CHAMP1 complex at telomeres in ALT U2OS cells. Notably, we observed a strong colocalization of CHAMP1 and POGZ with telomere foci, particularly with large telomere foci, in U2OS cells (**Extended Data Fig.3a,b**). This suggests that the CHAMP1 complex may play a role in promoting the formation of telomere clusters. DSBs at telomeres are known to initiate long-range movements and clustering of telomeres, and these processes are critical for homology-directed telomere synthesis[50]. Accordingly, we evaluated the response of U2OS cells to engineered DSBs at telomeres, using the TRF1-FokI[50,51]. TRF1-FokI induced telomeric DSBs (**Extended Data Fig.3c,d**), resulting in telomere clustering (**Fig. 3a,b**), as measured by an increase in the average size of telomere foci in ALT cells and a decrease in the total number [50] (**Fig. 3c,d**). Interestingly, this DSB-induced telomere clustering was significantly diminished in CHAMP1 or POGZ knockout U2OS cells (**Fig. 3c,d**). Depletion of CHAMP1 or POGZ also led to a decrease in the hallmarks of ALT recombination, including a reduction in ALT-associated PML bodies (APBs)[14,52] (**Fig. 3e,f**), which are sites of telomeric clustering and recombination[15,53], and a decrease of non-S phase telomeric DNA synthesis[16] (**Fig. 3g-i**). Taken together, our results demonstrate that the CHAMP1 complex plays a critical role in facilitating damage-induced telomere clustering and in maintaining ALT activity (**Fig. 3j**).

CHAMP1 complex promotes HDR at ALT telomeres

We next used the PICh (Proteomics of Isolated Chromatin Segments) method to identify the recruitment of telomere-associated proteins following DSBs, in the presence or absence of the CHAMP1 heterochromatin complex (**Fig. 4a and Extended Data Fig. 4a**). Consistent with

198 previous observations[51], multiple DNA repair- and telomere maintenance-related biological
199 processes were significantly upregulated at telomeres following TRF1-FokI induction (**Extended**
200 **Data Fig. 4b**). CRISPR knockout of CHAMP1 resulted in a decrease of other CHAMP1
201 complex proteins (i.e., POGZ and HP1α) at telomeres with DSBs, as well as a decrease of many
202 proteins associated with HR (e.g., RAD51, BRCA1, and BARD1), as measured by mass
203 spectrometry (**Fig. 4b**). These results are consistent with the known role of CHAMP1 and POGZ
204 in HR repair[34-36]. Additionally, CHAMP1 depletion also resulted in a reduction in proteins
205 involved in break-induced replication (BIR) or break-induced telomere synthesis (BITS) [51,54]
206 (i.e., POLD3, POLD4, RFC and PCNA) (**Fig. 4b**). Western blot analysis of PICh-purified
207 telomeres revealed an enrichment of the CHAMP1 complex (i.e., CHAMP1 and HP1α) and
208 BITS proteins (i.e., POLD3, RAD18 and PCNA) at telomeres in U2OS cells following TRF1-
209 FokI induction, but a reduction in CHAMP1-depleted U2OS cells (**Fig. 4c, lanes 9-12**).
210 Immunofluorescence further confirmed the reduction of CHAMP1 complex (i.e., POGZ and
211 HP1α) and H3K9me3 at telomeres in CHAMP1 knockout U2OS cells (**Fig. 4d-g and Extended**
212 **Data Fig. 4c,d**). Consistently, POGZ depletion also resulted in a reduction of proteins associated
213 with HR and BITS at telomeres with DSBs (**Extended Data Fig. 4e**). Consistent with the local
214 reduction in HR proteins, knockout of CHAMP1 or POGZ in U2OS cells resulted in a reduction
215 in HR activity at telomeres, as measured by RAD51 and pRPA2(S33) foci at damaged telomeres
216 (**Fig. 4h,i and Extended Data Fig. 4f,g**). Taken together, these results support a model in which
217 the CHAMP1 complex promotes HDR, potentially through the clustering of heterochromatin at
218 telomeres.
219
220 **CHAMP1 complex binds and recruits SETDB1 to telomeric heterochromatin clusters**
221 To further evaluate the regulation of telomere heterochromatin deposition, we examined
222 H3K9 methyltransferase levels and activity. Interestingly, SETDB1, but not other H3K9
223 methyltransferases, was recruited to telomeres after TRF1-FokI induction in U2OS cells,
224 whereas this recruitment was not observed in CHAMP1- and POGZ-depleted U2OS cells (**Fig.**
225 **5a**). Immunofluorescence confirmed the reduction in SETDB1 at telomeres following TRF1-
226 FokI induction in CHAMP1 or POGZ knockout U2OS cells (**Fig. 5b,c**). Based on previously
227 published data, indicating a POGZ and SETDB1 interaction[55], we reasoned that the CHAMP1
228 complex might directly recruit SETDB1 to telomeres. A strong interaction between SETDB1

229 and the Zn-fingers (type 2-7) of POGZ was predicted (iPTM =0.85) (**Fig. 5d**). Furthermore, an
230 N-terminal deletion of CHAMP1, causing loss of the interaction with POGZ, also exhibited
231 reduced interaction with SETDB1 (**Fig. 5e**). These results suggest that the CHAMP1 complex
232 may recruit SETDB1 to telomeres through POGZ (**Extended Data Fig. 5a**).
233 Recently, it has been shown that ALT activity relies on a high level of H3K9
234 trimethylation, facilitated by SETDB1, and on the recruitment of recombination factors [48].
235 Consistently, knockout of SETDB1 resulted in a decrease of H3K9me3 foci at telomeres
236 (**Extended Data Fig. 5b,c**). Importantly, SETDB1 depletion decreased CHAMP1 recruitment to
237 telomeres (**Fig. 5f,g**). Furthermore, SETDB1 depletion in U2OS cells led to reduced damage-
238 induced telomere clustering and APBs (**Fig. 5h,i**). Collectively, these findings suggest that the
239 CHAMP1 heterochromatin complex recruits SETDB1, thereby promoting a positive feedback
240 loop that enhances the formation of telomere heterochromatin clusters (**Fig. 5j**).
241
242 **CHAMP1 and HP1α are epistatic in the regulation of heterochromatin clustering**
243 Since HP1α is a critical subunit of the CHAMP1 heterochromatin complex, we next
244 examined its role in the regulation of telomeric HR and clustering. Consistent with previous
245 findings, HP1α is required for APBs formation[56]. HP1α knockdown resulted in a significant
246 decrease of damage-induced telomere clustering and APBs formation (**Fig. 6a,b and Extended**
247 **Data Fig. 6a**). HP1α knockdown did not result in a further decrease in damage-induced
248 telomere clustering and APBs in CHAMP1 knockout U2OS cells (**Fig. 6a,b and Extended Data**
249 **Fig. 6a**), indicating that CHAMP1 and HP1α are epistatic for APB formation and telomere
250 clustering. Consistent with the requirement of HP1α dimerization in the function of the
251 CHAMP1 complex, the wild-type HP1α protein, but not the HP1α-I165E dimerization mutant,
252 restored telomere clustering and APBs in cells with an HP1α knockdown (**Fig. 6c,d and**
253 **Extended Data Fig. 6b**). Furthermore, the C-terminal deletion mutant of CHAMP1, which lacks
254 HP1α binding, and the N-terminus deletion mutant of CHAMP1, which lacks POGZ binding, did
255 not restore RAD51 foci at telomeres or telomere clustering after CHAMP1 depletion (**Fig. 6e,f**
256 **and Extended Data Fig. 6c**). These findings highlight the critical importance of the multi-
257 subunit CHAMP1 heterochromatin complex in telomeric HR and clustering.
258
259

REV7 binding is not required for heterochromatin clustering or functional HR repair

The interaction of CHAMP1 and REV7 appears to be dispensable for the telomere HR and clustering (**Fig. 6e,f and Extended Data Fig. 6c**). REV7 does not co-immunoprecipitate with the CHAMP1 complex (**Fig. 1e,g,h**). Moreover, the CHAMP1-2A mutant protein, which has a disruption of the CHAMP1 binding site for REV7, can still assemble into the CHAMP1 complex, promote heterochromatin cluster formation, and promote HR activity (ie, RAD51 foci at sties of DSBs) (**Fig. 6e,f and Extended Data Fig. 6c).** Taken together, these results demonstrate that the activity of the REV7-independent CHAMP1 heterochromatin complex is essential for heterochromatic clustering and HR repair in heterochromatin.

Patients with CHAMP1 syndrome display impaired heterochromatin clustering and defects in HR repair

We next examined EBV-immortalized lymphoblast cell lines derived from patients with CHAMP1 syndrome, resulting from an inherited mutation in one allele of the *CHAMP1* gene. The cells were obtained via the Coriell mutant cell line repository (**Fig. 7**). These cell lines express the mutant (truncated) CHAMP1 proteins (**Fig. 7a, and Extended Data Fig. 7**), as predicted by their genomic sequencing. These truncated proteins, lacking the C-terminal HP1α binding domain, may act as dominant negative proteins or lead to haploinsufficiency. Interestingly, these CHAMP1 patient-derived cell lines exhibit a defect in heterochromatin clustering, as indicated by a decrease of H3K9me3 foci (**Fig. 7b,c**) compared to wild-type control cells. The CHAMP1 patient-derived cell lines also have a defect in RAD51 foci assembly following IR (**Fig. 7d,e**), consistent with a deficiency in HR, and exhibit heightened sensitivity to both IR and PARP inhibitors (**Fig. 7f,g**). In summary, lymphocytes from individuals carrying CHAMP1 mutations exhibit a defect in heterochromatin clustering and deficiencies in homologous recombination, providing a possible functional diagnostic assay for the CHAMP1 syndrome.

DISCUSSION

Taken together, our studies show that the CHAMP1 heterochromatin complex, consisting of CHAMP1, POGZ, and HP1α, has a direct role in heterochromatin assembly and Homology-Directed DNA Repair. The complex binds to H3K9me3 in heterochromatin sites, including

291 centromeres and telomeres, and contributes to the H3K9 trimethylation at these sites. The
292 complex is also recruited to heterochromatic sites with DSBs generated by ionizing radiation.
293 Moreover, the CHAMP1 heterochromatin complex plays a role in HDR at these heterochromatic
294 sites.

295 Our results support the presence of two distinct CHAMP1/POGZ complexes. One is
296 REV7-dependent, and the other is REV7-independent. We previously showed that the
297 CHAMP1/POGZ complex promotes HR by binding to REV7 and limiting the binding of REV7
298 to proteins in the Shieldin complex (i.e., the REV7, SHLD1, SLD2, SHLD3 complex). The
299 Shieldin complex is known to block the resection of DSB double strand breaks and thereby limit
300 the level of HR repair. While this HR mechanism primarily occur in euchromatic regions, it may
301 also occur to some extent in heterochromatic regions. However, in the current study, we identify
302 another CHAMP1 complex, the CHAMP1 heterochromatin complex, whose function was
303 previously unknown. This latter complex is enriched in heterochromatin and excludes the
304 CHAMP1 binding partner REV7. Here, we show that this complex interacts directly with
305 HP1α and promotes the H3K9me3 marks in heterochromatin. Moreover, this complex includes
306 the SETDB1 methyltransferase. The complex is required for the recruitment of HDR proteins to
307 heterochromatic regions of the chromosome. Loss of the CHAMP1 heterochromatin complex
308 results in a decrease in repair of TRF1-FokI mediated DSBs at telomeres. Knockdown of
309 CHAMP1 complex subunits, or mutation of individual subunits preventing complex assembly,
310 reduced pRPA and RAD51 foci at these sites.

311 Evaluation of the CHAMP1-2A mutant protein, which fails to bind to REV7[36] is
312 especially informative. CHAMP1-2A protein does not enable HDR repair by preventing the
313 binding of REV7 with the Shieldin complex[36]. However, the CHAMP1-2A mutant protein is still
314 functional for HDR repair through its interaction with the CHAMP1 heterochromatin complex.
315 As a subunit of the CHAMP1 heterochromatin complex, the CHAMP1-2A mutant protein still
316 allows heterochromatin clustering, recruitment of HDR proteins to heterochromatin, and repair
317 of DSBs in heterochromatin (i.e., formation of RAD51 foci).

318 Our study also demonstrates that the CHAMP1 heterochromatin complex is especially
319 important to heterochromatin clustering and HDR repair at specific heterochromatic sites. For
320 instance, the telomeres of ALT tumor cells are known to have high levels of H3K9me3, high
321 HDR activity, and high levels of replication stress. ALT telomeres appear to have a unique

322 heterochromatin environment [48,57]. The CHAMP1 heterochromatin complex is required for
323 assembly and maintenance of ALT telomeres, and knockdown or knockout of the CHAMP1
324 complex results in decreased DSB-induced telomere cluster formation and reduced HDR activity,
325 coincident with a loss of telomere-associated histone H3 lysine 9 trimethylation (H3K9me3).
326 The CHAMP1 heterochromatin complex may play additional roles in heterochromatin structures.
327 For instance, the complex may be regulated by the ATM kinase[2] or may function in HDR repair
328 at the periphery of the cell nuclease[9,18]. The complex may play a role in specific signaling
329 events required for assembling heterochromatin at stressed replication forks[58,59]. Future studies
330 will be required to assess the role of the CHAMP1 heterochromatin complex at these other
331 heterochromatic sites.

332 A reduction in H3K9me3 is known to result from a mislocalization or inactivation of the
333 SETDB1, a methyltransferase known to trimethylate H3K9[60]. Consistent with these findings,
334 our AF2 analysis, immunoprecipitation studies, and PICh results revealed an interaction of
335 SETDB1 with the POGZ subunit of the complex, required for the recruitment of SETDB1 to
336 sites of heterochromatin. Taken together, the CHAMP1 complex appears to be a critical
337 determinant of heterochromatin clustering. Genetic ablation of a subunit of the complex, or a
338 mutation in a subunit which disrupts complex assembly, results in failure to recruit SETDB1 and
339 in loss of heterochromatin clustering.

340 Previous studies have suggested that tightly-packed heterochromatin regions have an
341 overall decrease in HDR activity[3]. Paradoxically, in our studies and in other recent reports[48,61,62],
342 the increase in H3K9 trimethylation or other modifications in the heterochromatin composition at
343 telomeres, may enhance HDR activity. Consistent with these findings, the CHAMP1 complex
344 may promote HDR by functioning as a bridge between two heterochromatin nucleosomes, either
345 intra- or interchromosomally, through its interaction with H3K9me3 in heterochromatin. This
346 bridge may facilitate the formation of heterochromatin clusters, thereby creating an environment
347 that promotes the recruitment and stabilization of HDR proteins.

348 Finally, individuals with *de novo* heterozygous mutations in *CHAMP1*, known as
349 CHAMP1 syndrome, present with a neurodevelopmental disorder characterized by intellectual
350 disability, behavioral symptoms, and distinct dysmorphic features. Interestingly, *de novo*
351 heterozygous mutations in the *POGZ* gene also result in another rare but highly-related
352 neurodevelopment syndrome called the White Sutton Syndrome (WSS) [25,27,28,30,31,63]. The

mutant proteins encoded by pathogenic alleles of CHAMP1 have C-terminus truncations, and perhaps dominant negative activity, and cannot assemble into functional CHAMP1 complexes. Accordingly, lymphoblast cultures derived from individuals with CHAMP1 syndrome and expressing these mutant proteins have defects in heterochromatin and homologous recombination. These functional defects may also underlie the neurodevelopmental defects in these individuals. Lymphoblasts from these individuals have phenotypic characteristics similar to engineered human cells lacking the CHAMP1 complex. Taken together, these cellular characteristics could serve as a functional diagnostic screening tool for identifying individuals with CHAMP1 syndrome among the much larger number of individuals with autism spectrum disorders. In conclusion, we provide evidence that the CHAMP1 heterochromatin complex is critical for the heterochromatin HDR repair, not only in tumor cells but also in normal tissue cells. The clinical significance of the CHAMP1 complex will require further studies.

Figure Legends

Fig. 1. CHAMP1-POGZ-HP1α form a REV7 independent heterochromatin complex. a. AlphaFold2-Multimer (AF2)-predicted structural model of POGZ_Cter (peach)-CHAMP1_NZnF (cyan) complex. The key residues (shown in sticks) contributing to the protein-protein interactions are highlighted in the inset including CHAMP1 residues (Q56, L61 and T70) that are mutated to disrupt the interaction between POGZ and CHAMP1. **b**. The AF2-predicted model of POGZ_Cter-CHAMP1_NZnF is colored based on the confidence in the model prediction (100-high (blue) and 50-low (red)) and corresponding predicted aligned error plot (PAE) matrix showing the confidence in the predicted interaction between CHAMP1_NZnF and POGZ_Cter domains along with interface-predicted template scores (iPTM) for the AF2 prediction. **c.** (Top) Schematic of CHAMP1 wild-type (WT) and mutants. N-ZNFs (N-terminus C2H2-Zn finger domains), SPE (PxxSPExxK motifs), WK (SPxxWKxxP motifs), FPE (FPExxK motifs), C-ZNFs (C-terminus C2H2-Zn finger domains), and SBM (REV7 seatbelt-binding motif). 2A indicates W334A/K335A mutant. (Bottom) Schematic of CHAMP1 complex connecting two H3K9me3 sites. The N-terminus of CHAMP1 binds to the C-terminus of POGZ. Additionally, both the C-terminus of CHAMP and the HPZ motif of POGZ can independently bind to HP1α. CHAMP1 shows a preference for binding to the HP1α dimer, while POGZ is capable of binding to either the HP1α dimer or monomer. N-terminus of HP1α directly interacts with H3K9me3. **d**. Western blot showing GFP-immunoprecipitation of GFP-empty vector, GFP-CHAMP1 WT or N- or C- terminal deletion mutants, and the co-immunoprecipitation of endogenous POGZ, HP1α and REV7. **e.** Western blot showing GFP-immunoprecipitation of GFP-empty vector, GFP-CHAMP1 WT and GFP-CHAMP1 mutants in 293T cells, and the co-immunoprecipitation of endogenous POGZ, HP1α and REV7. **f**. Western blot showing GFP-immunoprecipitation of GFP-empty vector, GFP-HP1α WT or I165E mutant, and the co-immunoprecipitation of endogenous POGZ, CHAMP1 and H3K9me3. GAPDH acts as a negative control. **g.** Western blot showing GFP-immunoprecipitation of GFP-empty vector, GFP-HP1α in 293T WT and sgCHAMP1 cells, and the co-immunoprecipitation of endogenous POGZ, CHAMP1, REV7 and H3K9me3. GAPDH acts as negative control for IP. **h.** Western blot

s
h
o
w
i

Fig. 2. The CHAMP1 complex is required for the nuclear distribution of H3K9me3. a. Representative immunofluorescence (IF) confocal images of the colocalized CHAMP1 and H3K9me3 foci with/without IR (5Gy) treatment in U2OS cells. DAPI was used to stain the nuclei. Scale bar, 5 µm. **b**. Square analysis of the intensity and colocalization of H3K9me3 and CHAMP1 foci. **c**. Representative IF images of H3K9me3 foci in WT, sgCHAMP1 and sgPOGZ U2OS cells. DAPI was used to stain the nuclei. Scale bar, 5 µm. **d**. Quantification of H3K9me3 foci in (c). Error bars indicate SEM. More than 100 cells were counted. ****P<0.0001. Statistical analysis was performed using two-tailed Student's t test. **e**. Representative IF images of HP1α foci in WT, sgCHAMP1 and sgPOGZ U2OS cells. DAPI was used to stain the nuclei. Scale bar, 5 µm. **f**. Quantification of HP1α foci in (e). Error bars indicate SEM. More than 100 cells were counted. ****P<0.0001. Statistical analysis was performed using two-tailed Student's ttest. **g**. Representative IF-FISH confocal images of H3K9me3 colocalization with centromere (Cent) in WT, sgCHAMP1 and sgPOGZ U2OS cells. DAPI was used to stain the nuclei. Scale

p
r
e
c
i
p

bar, 5 µm. **h**. Quantification of H3K9me3-Centromere colocalizations in (g). Error bars indicate SEM. More than 100 cells were counted. ****P<0.0001. Statistical analysis was performed using two-tailed Student's t test. **i**. Representative IF confocal images of H3K9me3-TRF2 colocalization in WT, sgCHAMP1 and sgPOGZ U2OS cells. TRF2 was used as a telomere maker. DAPI was used to stain the nuclei. Scale bar, 5 µm. **j**. Quantification of H3K9me3 colocalization with TRF2 in (i). Error bars indicate SEM. More than 100 cells were counted. ****P<0.0001. Statistical analysis was performed using two-tailed Student's t test. **k**. ChIP-qPCR analyses showing relative enrichment levels of H3 (Top) and H3K9me3 (Bottom) at telomeres. Level of H3K9me3 was normalized to total H3 levels (H3K9me3/H3). Error bars indicate SD. P-values calculated using Student's T-test (***P<0.001; ns, non-significant).

Fig. 3. The CHAMP1 Complex promotes break-induced telomere clustering and synthesis. **a**. Schematic of U2OS-TRF1-FokI cell and time course of IF/FISH following Dox/4-OHT treatment. **b**. Representative FISH confocal images with telomere probe (green) treated with/without TRF1-FokI in U2OS cells. DAPI was used to stain the nuclei. Scale bar, 5 µm. **c-d**. CHAMP1 and POGZ KO U2OS cells were examined by telomere FISH after TRF1-FokI treatment (a). Average telomere (Telo) foci size (c) and telomere number (d) per nucleus was calculated using ImageJ. Error bars indicate SEM. More than 100 cells were counted. ****P<0.0001. Statistical analysis was performed using two-tailed Student's t test. **e**. PML immunostaining combined with telomere FISH in wild-type (WT), sgCHAMP1 and sgPOGZ U2OS cells after TRF1-FokI treatment (a). Colocalization of PML foci and telomere signals (APBs) are shown as indicated. DAPI was used to stain the nuclei. Scale bar, 5 µm. **f**. Quantification of APBs shown in (e). Error bars indicate SEM. More than 100 cells were counted. ****P<0.0001. Statistical analysis was performed using two-tailed Student's t test. **g**. Schematic of U2OS-TRF1-FokI cell and time course of IF assay following Dox/4-OHT and EdU treatment. **h**. Representative confocal images of immunostaining of TRF2 and EdU foci in S phase and non-S phase of U2OS cells following the treatment in (g). DAPI was used to stain the nuclei. Scale bar, 5 µm. **i**. Quantification of the colocalized TRF2 and EdU foci in WT, sgCHAMP1 and sgPOGZ U2OS cells. Error bars indicate SEM. More than 100 cells were counted. ****P<0.0001. Statistical analysis was performed using two-tailed Student's t test. **j.** A cartoon showing that CHAMP1 complex promotes telomere clustering, APBs formation and facilitates Break-induced new telomeric DNA synthesis.

Fig. 4. The CHAMP1 complex establishes telomeric heterochromatin and promotes the recruitment of HR and BIR factors. a. Schematic of the PICh approach used to define the telomere specific proteome in WT and sgCHAMP1 U2OS cells after TRF1-FokI (-/+Dox/4-OHT) treatment. Fractionated and precleared chromatin was hybridized to a biotinylated telomeric probe and subsequently captured on magnetic beads. Telomere-associated proteins were analyzed by silver staining, western blot analysis and mass spectrometry. PFA, paraformaldehyde. **b.** Scatterplot of the telomere specific DSB response proteome profile enriched by PICh in wild-type (WT) and sgCHAMP1 U2OS cells induced with TRF1-FokI. Mass Spectrometry data was shown in Table S1. Scatterplot of log2 FC[(+Dox+1)/(-Dox+1) of total peptide number] from two independent experiments. FC, fold change. Homologous recombination (HR) pathway proteins with Log2 FC > 1 in WT were highlighted in red. Break-

520 induced replication (BIR) pathway proteins with Log2 FC > 1 in WT were highlighted in green.
521 CBX5 (HP1α) was highlighted in blue. The red dotted line indicates the same value of log2
522 FC(+Dox/-Dox) in both WT and sgCHAMP1 cells. **c.** Western blot from PICh experiments in
523 U2OS with/without Dox-induced TRF1-FokI. Telomere-associated proteins are blotted with the
524 indicated antibodies. **d**. Representative IF confocal images depicting the colocalization of HP1α
525 (Green) with TRF1-FokI (T1-F1, mCherry tagged, Red) in WT and sgCHAMP1 U2OS cells
526 induced with/without TRF1-FokI for 2 hours. DAPI (blue) was used to stain the nuclei. Scale
527 bar, 5 µm. **e**. Quantification of HP1α-TRF1-FokI colocalization events in (d). Error bars indicate
528 SEM. More than 100 cells were counted. ****P<0.0001. Statistical analysis was performed
529 using two-tailed Student's t test. **f**. Representative IF confocal images depicting the
530 colocalization of H3K9me3 (Green) with TRF1-FokI (T1-F1, mCherry tagged, Red) in WT and
531 sgCHAMP1 U2OS cells induced with/without TRF1-FokI for 2 hours. DAPI (blue) was used to
532 stain the nuclei. Scale bar, 5 µm. **g**. Quantification of H3K9me3-TRF1-FokI colocalization
533 events in (f). Error bars indicate SEM. More than 100 cells were counted. ****P<0.0001.
534 Statistical analysis was performed using two-tailed Student's t test. **h**. Representative IF confocal
535 images depicting the colocalization of RAD51 (Green) with TRF1-FokI (T1-F1, mCherry
536 tagged, Red) in WT, sgCHAMP1 and sgPOGZ U2OS cells induced with/without TRF1-FokI for
537 2 hours. DAPI (blue) was used to stain the nuclei. Scale bar, 5 µm. **i**. Quantification of RAD51-
538 TRF1-FokI colocalization events in (h). Error bars indicate SEM. More than 100 cells were
539 counted. ****P<0.0001. Statistical analysis was performed using two-tailed Student's t test.
540
541
542 **Fig. 5. The CHAMP1 complex promotes the recruitment of SETDB1 to telomeres. a.**
543 Scatterplot of Log2 (+Dox+1)/(-Dox+1) of total peptide number from the telomere specific DSB
544 response proteome profile enriched by PICh in wild-type (WT), sgCHAMP1 and sgPOGZ U2OS
545 cells induced with TRF1-FokI. Mass Spectrometry data was shown in Table S2. SETDB1 is
546 highlighted. **b**. Representative IF confocal images of SETDB1 (Green) colocalization with
547 telomeres with double-strand breaks (T1-F1, mCherry, Red) in wild-type (WT), sgCHAMP1 and
548 sgPOGZ U2OS cells induced with TRF1-FokI for 2 h. Arrow indicates SETDB1 and TRF1-FokI
549 colocalization. DAPI was used to stain the nuclei. Scale bar, 5 µm. **c**. Quantification of (a) for
550 number of SETDB1-mCherry colocalization events. Error bars indicate SEM. More than 100
551 cells were counted. ****P<0.0001. Statistical analysis was performed using two-tailed Student's
552 t test. **d.** (Top) AlphaFold2-Multimer (AF2)-predicted structural model of POGZ_ZnFcore
553 (peach)-SETDB1_Cter (cyan) complex. The key residues (shown in sticks) contributing to the
554 protein-protein interactions are highlighted in the inset including residues (C532, C535, H548
555 and H534) from POGZ_ZnFcore potentially forming a C2H2-type Zn finger that could be
556 critical in maintaining interaction between POGZ and SETDB1. (Bottom) The AF2-predicted
557 model of POGZ_ZnFcore-SETDB1_Cter complex is colored based on the confidence in the
558 model prediction (100-high (blue) and 50-low (red)) and corresponding PAE matrix showing the
559 confidence in the predicted interaction between POGZ_ZnFcore and SETDB1_Cter domains
560 along with iPTM socres for the AF2 prediction. **e.** Western blot showing GFP-
561 immunoprecipitation of GFP-vector control, GFP-CHAMP1 WT or deletion mutants, and the co-
562 immunoprecipitation of endogenous SETDB1 and POGZ. GAPDH acts as a negative control for
563 IP. **f.** Representative IF-FISH confocal images of CHAMP1 colocalization with telomeres in
564 wild-type (WT) and sgSETDB1 U2OS cells. Arrow indicates CHAMP1-telomere colocalization.
565 DAPI (blue) was used to stain the nuclei. Scale bar, 5 µm. **g**. Quantification of (f) for number of

CHAMP1-telomere colocalization events. Error bars indicate SEM. More than 100 cells were counted. ****P<0.0001. Statistical analysis was performed using two-tailed Student's t test. **h**. SETDB1 KO TRF1-FokI U2OS cells were examined by FISH using a FITC-labeled telomere probe after DOX/4-OHT treatment. Average telomere foci size per nucleus was calculated using ImageJ. Error bars indicate SEM. More than 100 cells were counted. ****P<0.0001. Statistical analysis was performed using two-tailed Student's t test. **i**. PML immunostaining combined with telomere FISH in SETDB1 KO U2OS cells after DOX/4-OHT treatment. Colocalization of PML foci and telomere signals (APBs) are shown. Error bars indicate SEM. More than 100 cells were counted. ****P<0.0001. Statistical analysis was performed using two-tailed Student's t test. **j.** A cartoon showing that the recruitment of SETDB1 by CHAMP1 complex could potentially facilitates a positive feedback loop that boosts the formation of telomere heterochromatin clusters.

Fig. 6. HP1α and CHAMP1 are epistatic in the regulation of telomeric HR and clustering. a-b. Wild-type (WT) and sgCHAMP1 U2OS-TRF1-FokI cells were treated with siControl or siHP1α, followed by examination of FISH using a telomere probe, or PML combined with telomere IF-FISH staining after DOX/4-OHT treatment. (a) Average telomere foci size per nucleus was calculated using ImageJ. Error bars indicate SEM. More than 100 cells were counted. ****P<0.0001, **P<0.01. Statistical analysis was performed using two-tailed Student's t test. (b) Quantification of colocalization of PML foci and telomere signals (APBs). Error bars indicate SEM. More than 100 cells were counted. ****P<0.0001, **P<0.01. Statistical analysis was performed using two-tailed Student's t test. **c-d.** WT, sgHP1α, and sgHP1α U2OS cells with ectopically expressed HP1α WT or mutant I165E were examined with FISH using a telomere probe, or PML combined with telomere IF-FISH staining using a FITC-labeled telomere probe after DOX/4-OHT treatment. (c) Average telomere foci size per nucleus was calculated using ImageJ. Error bars indicate SEM. More than 100 cells were counted. ****P<0.0001. Statistical analysis was performed using two-tailed Student's t test. (d) Quantification of colocalization of PML foci and telomere signals (APBs). Error bars indicate SEM. More than 100 cells were counted. ****P<0.0001. Statistical analysis was performed using two-tailed Student's t test. **e-f.** WT, sgCHAMP1, and sgCHAMP1 U2OS cells with ectopically expressed CHAMP1 WT or mutants (ΔN, 2A and ΔC) were examined with IF using anti-RAD51 or FISH using a telomere probe. (e) Quantification of RAD51-TRF1-FokI colocalization events. Error bars indicate SEM. More than 100 cells were counted. ****P<0.0001. Statistical analysis was performed using two-tailed Student's t test. (f) Average telomere foci size per nucleus was calculated using ImageJ. Error bars indicate SEM. More than 100 cells were counted. ****P<0.0001, **P<0.01. Statistical analysis was performed using two-tailed Student's t test.

Fig. 7. Peripheral blood lymphocytes from Patients with CHAMP1 syndrome display impaired heterochromatin clustering and defects in HR repair. a. Schematic of CHAMP1 mutants from patients with CHAMP1 syndrome. **b**. EBV-immortalized lymphoblast cell lines derived from several CHAMP1 patients (Coriell) were examined by immunostaining with H3K9me3 antibody. Representative images show the H3K9me3 foci. DAPI was used to stain the nuclei. Scale bar, 5 μm. **c**. Quantification of H3K9me3 foci of the CHAMP1 patient lymphoblast cells in (b). More than 100 cells were counted. ****P<0.0001. Statistical analysis was performed

using one-way ANOVA. **d**. Representative images of RAD51 foci formation in normal and CHAMP1 patient lymphoblast cells following with/without 5Gy IR treatment. DAPI was used to stain the nuclei. Scale bar, 5 µm. **e**. Quantification of RAD51 foci of the CHAMP1 patient lymphoblast cells following with 5Gy IR treatment. More than 100 cells were counted. ****P<0.0001. Statistical analysis was performed using one-way ANOVA. **f**. 3-day cytotoxicity analysis of the normal and CHAMP1 patient lymphoblast cells treated with various dose of radiation. Cell viability was detected by CellTiter Glo (Promega). Error bars indicate SD, n=3 independent experiments. **g**. 3-day cytotoxicity analysis of the normal and CHAMP1 patient lymphoblast cells treated with various dose of Olaparib. Cell viability was detected by CellTiter Glo (Promega). Error bars indicate SD, n=3 independent experiments.

References

1 Dabin, J., Giacomini, G., Petit, E. & Polo, S. E. New facets in the chromatin-based regulation of genome maintenance. *DNA Repair (Amst)* **140**, 103702 (2024). https://doi.org/10.1016/j.dnarep.2024.103702

2 Goodarzi, A. A. *et al.* ATM signaling facilitates repair of DNA double-strand breaks associated with heterochromatin. *Mol Cell* **31**, 167-177 (2008). https://doi.org/10.1016/j.molcel.2008.05.017

3 Price, B. D. & D'Andrea, A. D. Chromatin remodeling at DNA double-strand breaks. *Cell* **152**, 1344-1354 (2013). https://doi.org/10.1016/j.cell.2013.02.011

4 Watts, F. Z. Repair of DNA Double-Strand Breaks in Heterochromatin. *Biomolecules* **6** (2016). https://doi.org/10.3390/biom6040047

5 Bannister, A. J. *et al.* Selective recognition of methylated lysine 9 on histone H3 by the HP1 chromo domain. *Nature* **410**, 120-124 (2001). https://doi.org/10.1038/35065138

6 Padeken, J., Methot, S. P. & Gasser, S. M. Establishment of H3K9-methylated heterochromatin and its functions in tissue differentiation and maintenance. *Nat Rev Mol Cell Biol* **23**, 623-640 (2022). https://doi.org/10.1038/s41580-022-00483-w

7 Hyun, K., Jeon, J., Park, K. & Kim, J. Writing, erasing and reading histone lysine methylations. *Exp Mol Med* **49**, e324 (2017). https://doi.org/10.1038/emm.2017.11

8 Chiolo, I. *et al.* Double-strand breaks in heterochromatin move outside of a dynamic HP1a domain to complete recombinational repair. *Cell* **144**, 732-744 (2011). https://doi.org/10.1016/j.cell.2011.02.012

9 Jakob, B. *et al.* DNA double-strand breaks in heterochromatin elicit fast repair protein recruitment, histone H2AX phosphorylation and relocation to euchromatin. *Nucleic Acids Res* **39**, 6489-6499 (2011). https://doi.org/10.1093/nar/gkr230

10 Noon, A. T. *et al.* 53BP1-dependent robust localized KAP-1 phosphorylation is essential for heterochromatic DNA double-strand break repair. *Nat Cell Biol* **12**, 177-184 (2010). https://doi.org/10.1038/ncb2017

11 Ryu, T. *et al.* Heterochromatic breaks move to the nuclear periphery to continue recombinational repair. *Nat Cell Biol* **17**, 1401-1411 (2015). https://doi.org/10.1038/ncb3258

12 Tsouroula, K. *et al.* Temporal and Spatial Uncoupling of DNA Double Strand Break Repair Pathways within Mammalian Heterochromatin. *Mol Cell* **63**, 293-305 (2016). https://doi.org/10.1016/j.molcel.2016.06.002

13 Dilley, R. L. & Greenberg, R. A. ALTernative Telomere Maintenance and Cancer. *Trends Cancer* **1**, 145-156 (2015). https://doi.org/10.1016/j.trecan.2015.07.007

14 Henson, J. D., Neumann, A. A., Yeager, T. R. & Reddel, R. R. Alternative lengthening of telomeres in mammalian cells. *Oncogene* **21**, 598-610 (2002). https://doi.org/10.1038/sj.onc.1205058

15 Draskovic, I. *et al.* Probing PML body function in ALT cells reveals spatiotemporal requirements for telomere recombination. *Proc Natl Acad Sci U S A* **106**, 15726-15731 (2009). https://doi.org/10.1073/pnas.0907689106

16 Zhang, J. M., Yadav, T., Ouyang, J., Lan, L. & Zou, L. Alternative Lengthening of Telomeres through Two Distinct Break-Induced Replication Pathways. *Cell Rep* **26**, 955-968 e953 (2019). https://doi.org/10.1016/j.celrep.2018.12.102

17 Vermeulen, M. *et al.* Quantitative interaction proteomics and genome-wide profiling of epigenetic histone marks and their readers. *Cell* **142**, 967-980 (2010). https://doi.org/10.1016/j.cell.2010.08.020

18 Itoh, G. *et al.* CAMP (C13orf8, ZNF828) is a novel regulator of kinetochore-microtubule attachment. *EMBO J* **30**, 130-144 (2011). https://doi.org/10.1038/emboj.2010.276

19 Nozawa, R. S. *et al.* Human POGZ modulates dissociation of HP1alpha from mitotic chromosome arms through Aurora B activation. *Nat Cell Biol* **12**, 719-727 (2010). https://doi.org/10.1038/ncb2075

20 Garrity, M. *et al.* Neurodevelopmental phenotypes in individuals with pathogenic variants in CHAMP1. *Cold Spring Harb Mol Case Stud* **7** (2021). https://doi.org/10.1101/mcs.a006092

21 Hempel, M. *et al.* De Novo Mutations in CHAMP1 Cause Intellectual Disability with Severe Speech Impairment. *Am J Hum Genet* **97**, 493-500 (2015). https://doi.org/10.1016/j.ajhg.2015.08.003

22 Isidor, B. *et al.* De Novo Truncating Mutations in the Kinetochore-Microtubules Attachment Gene CHAMP1 Cause Syndromic Intellectual Disability. *Hum Mutat* **37**, 354-358 (2016). https://doi.org/10.1002/humu.22952

23 Levy, T. *et al.* CHAMP1 disorder is associated with a complex neurobehavioral phenotype including autism, ADHD, repetitive behaviors and sensory symptoms. *Hum Mol Genet* **31**, 2582-2594 (2022). https://doi.org/10.1093/hmg/ddac018

24 Tanaka, A. J. *et al.* De novo pathogenic variants in CHAMP1 are associated with global developmental delay, intellectual disability, and dysmorphic facial features. *Cold Spring Harb Mol Case Stud* **2**, a000661 (2016). https://doi.org/10.1101/mcs.a000661

25 Dentici, M. L. *et al.* Expanding the phenotypic spectrum of truncating POGZ mutations: Association with CNS malformations, skeletal abnormalities, and distinctive facial dysmorphism. *Am J Med Genet A* **173**, 1965-1969 (2017). https://doi.org/10.1002/ajmg.a.38255

26 Duan, J. *et al.* White-Sutton syndrome and congenital heart disease: case report and literature review. *BMC Pediatr* **23**, 158 (2023). https://doi.org/10.1186/s12887-023-03972-9

27 Ferretti, A. *et al.* POGZ-related epilepsy: Case report and review of the literature. *Am J Med Genet A* **179**, 1631-1636 (2019). https://doi.org/10.1002/ajmg.a.61206

28 Fukai, R. *et al.* A case of autism spectrum disorder arising from a de novo missense mutation in POGZ. *J Hum Genet* **60**, 277-279 (2015). https://doi.org/10.1038/jhg.2015.13

29 Matsumura, K. *et al.* De novo POGZ mutations in sporadic autism disrupt the DNA-binding activity of POGZ. *J Mol Psychiatry* **4**, 1 (2016). https://doi.org/10.1186/s40303-016-0016-x

30 Tan, B. *et al.* A novel de novo POGZ mutation in a patient with intellectual disability. *J Hum Genet* **61**, 357-359 (2016). https://doi.org/10.1038/jhg.2015.156

31 Ye, Y. *et al.* De novo POGZ mutations are associated with neurodevelopmental disorders and microcephaly. *Cold Spring Harb Mol Case Stud* **1**, a000455 (2015). https://doi.org/10.1101/mcs.a000455

32 Zhao, W. *et al.* POGZ de novo missense variants in neuropsychiatric disorders. *Mol Genet Genomic Med* **7**, e900 (2019). https://doi.org/10.1002/mgg3.900

33 Zhao, W. *et al.* Rare inherited missense variants of POGZ associate with autism risk and disrupt neuronal development. *J Genet Genomics* **46**, 247-257 (2019). https://doi.org/10.1016/j.jgg.2019.04.002

34 Fujita, H. *et al.* CHAMP1-POGZ counteracts the inhibitory effect of 53BP1 on homologous recombination and affects PARP inhibitor resistance. *Oncogene* **41**, 2706-2718 (2022). https://doi.org/10.1038/s41388-022-02299-6

35 Heath, J. *et al.* POGZ promotes homology-directed DNA repair in an HP1-dependent manner. *EMBO Rep* **23**, e51041 (2022). https://doi.org/10.15252/embr.202051041

36 Li, F. *et al.* CHAMP1 binds to REV7/FANCV and promotes homologous recombination repair. *Cell Rep* **40**, 111297 (2022). https://doi.org/10.1016/j.celrep.2022.111297

37 Dev, H. *et al.* Shieldin complex promotes DNA end-joining and counters homologous recombination in BRCA1-null cells. *Nat Cell Biol* **20**, 954-965 (2018). https://doi.org/10.1038/s41556-018-0140-1

38 Ghezraoui, H. *et al.* 53BP1 cooperation with the REV7-shieldin complex underpins DNA structure-specific NHEJ. *Nature* **560**, 122-127 (2018). https://doi.org/10.1038/s41586-018-0362-1

39 Gupta, R. *et al.* DNA Repair Network Analysis Reveals Shieldin as a Key Regulator of NHEJ and PARP Inhibitor Sensitivity. *Cell* **173**, 972-988 e923 (2018). https://doi.org/10.1016/j.cell.2018.03.050

40 Mirman, Z. *et al.* 53BP1-RIF1-shieldin counteracts DSB resection through CST- and Polalpha-dependent fill-in. *Nature* **560**, 112-116 (2018). https://doi.org/10.1038/s41586-018-0324-7

41 Noordermeer, S. M. *et al.* The shieldin complex mediates 53BP1-dependent DNA repair. *Nature* **560**, 117-121 (2018). https://doi.org/10.1038/s41586-018-0340-7

42 Jumper, J. *et al.* Highly accurate protein structure prediction with AlphaFold. *Nature* **596**, 583-589 (2021). https://doi.org/10.1038/s41586-021-03819-2

43 Liu, J. *et al.* Enhancing alphafold-multimer-based protein complex structure prediction with MULTICOM in CASP15. *Commun Biol* **6**, 1140 (2023). https://doi.org/10.1038/s42003-023-05525-3

44 Brasher, S. V. *et al.* The structure of mouse HP1 suggests a unique mode of single peptide recognition by the shadow chromo domain dimer. *EMBO J* **19**, 1587-1597 (2000). https://doi.org/10.1093/emboj/19.7.1587

45 Machida, S. *et al.* Structural Basis of Heterochromatin Formation by Human HP1. *Mol Cell* **69**, 385-397 e388 (2018). https://doi.org/10.1016/j.molcel.2017.12.011

46 Palm, W. & de Lange, T. How shelterin protects mammalian telomeres. *Annu Rev Genet* **42**, 301-334 (2008). https://doi.org/10.1146/annurev.genet.41.110306.130350

47 Cubiles, M. D. *et al.* Epigenetic features of human telomeres. *Nucleic Acids Res* **46**, 2347-2355 (2018). https://doi.org/10.1093/nar/gky006

48 Gauchier, M. *et al.* SETDB1-dependent heterochromatin stimulates alternative lengthening of telomeres. *Sci Adv* **5**, eaav3673 (2019). https://doi.org/10.1126/sciadv.aav3673

49 Udugama, M. *et al.* Mutations inhibiting KDM4B drive ALT activation in ATRX-mutated glioblastomas. *Nat Commun* **12**, 2584 (2021). https://doi.org/10.1038/s41467-021-22543-z

50 Cho, N. W., Dilley, R. L., Lampson, M. A. & Greenberg, R. A. Interchromosomal homology searches drive directional ALT telomere movement and synapsis. *Cell* **159**, 108-121 (2014). https://doi.org/10.1016/j.cell.2014.08.030

51 Zhang, T. *et al.* Break-induced replication orchestrates resection-dependent template switching. *Nature* **619**, 201-208 (2023). https://doi.org/10.1038/s41586-023-06177-3

52 Yeager, T. R. *et al.* Telomerase-negative immortalized human cells contain a novel type of promyelocytic leukemia (PML) body. *Cancer Res* **59**, 4175-4179 (1999).

53 Zhang, H. *et al.* Nuclear body phase separation drives telomere clustering in ALT cancer cells. *Mol Biol Cell* **31**, 2048-2056 (2020). https://doi.org/10.1091/mbc.E19-10-0589

54 Dilley, R. L. *et al.* Break-induced telomere synthesis underlies alternative telomere maintenance. *Nature* **539**, 54-58 (2016). https://doi.org/10.1038/nature20099

55 Sun, X. *et al.* POGZ suppresses 2C transcriptional program and retrotransposable elements. *Cell Rep* **42**, 112867 (2023). https://doi.org/10.1016/j.celrep.2023.112867

56 Jiang, W. Q. *et al.* Induction of alternative lengthening of telomeres-associated PML bodies by p53/p21 requires HP1 proteins. *J Cell Biol* **185**, 797-810 (2009). https://doi.org/10.1083/jcb.200810084

57 Hartlieb, S. A. *et al.* Alternative lengthening of telomeres in childhood neuroblastoma from genome to proteome. *Nat Commun* **12**, 1269 (2021). https://doi.org/10.1038/s41467-021-21247-8

58 Alabert, C. & Groth, A. Chromatin replication and epigenome maintenance. *Nat Rev Mol Cell Biol* **13**, 153-167 (2012). https://doi.org/10.1038/nrm3288

59 Gaggioli, V. *et al.* Dynamic de novo heterochromatin assembly and disassembly at replication forks ensures fork stability. *Nat Cell Biol* **25**, 1017-1032 (2023). https://doi.org/10.1038/s41556-023-01167-z

60 Wang, H. *et al.* mAM facilitates conversion by ESET of dimethyl to trimethyl lysine 9 of histone H3 to cause transcriptional repression. *Mol Cell* **12**, 475-487 (2003). https://doi.org/10.1016/j.molcel.2003.08.007

61 Shi, G. *et al.* A critical role of telomere chromatin compaction in ALT tumor cell growth. *Nucleic Acids Res* **48**, 6019-6031 (2020). https://doi.org/10.1093/nar/gkaa224

62 Voon, H. P. J., Collas, P. & Wong, L. H. Compromised Telomeric Heterochromatin Promotes ALTernative Lengthening of Telomeres. *Trends Cancer* **2**, 114-116 (2016). https://doi.org/10.1016/j.trecan.2016.02.003

63 White, J. *et al.* POGZ truncating alleles cause syndromic intellectual disability. *Genome Med* **8**, 3 (2016). https://doi.org/10.1186/s13073-015-0253-0

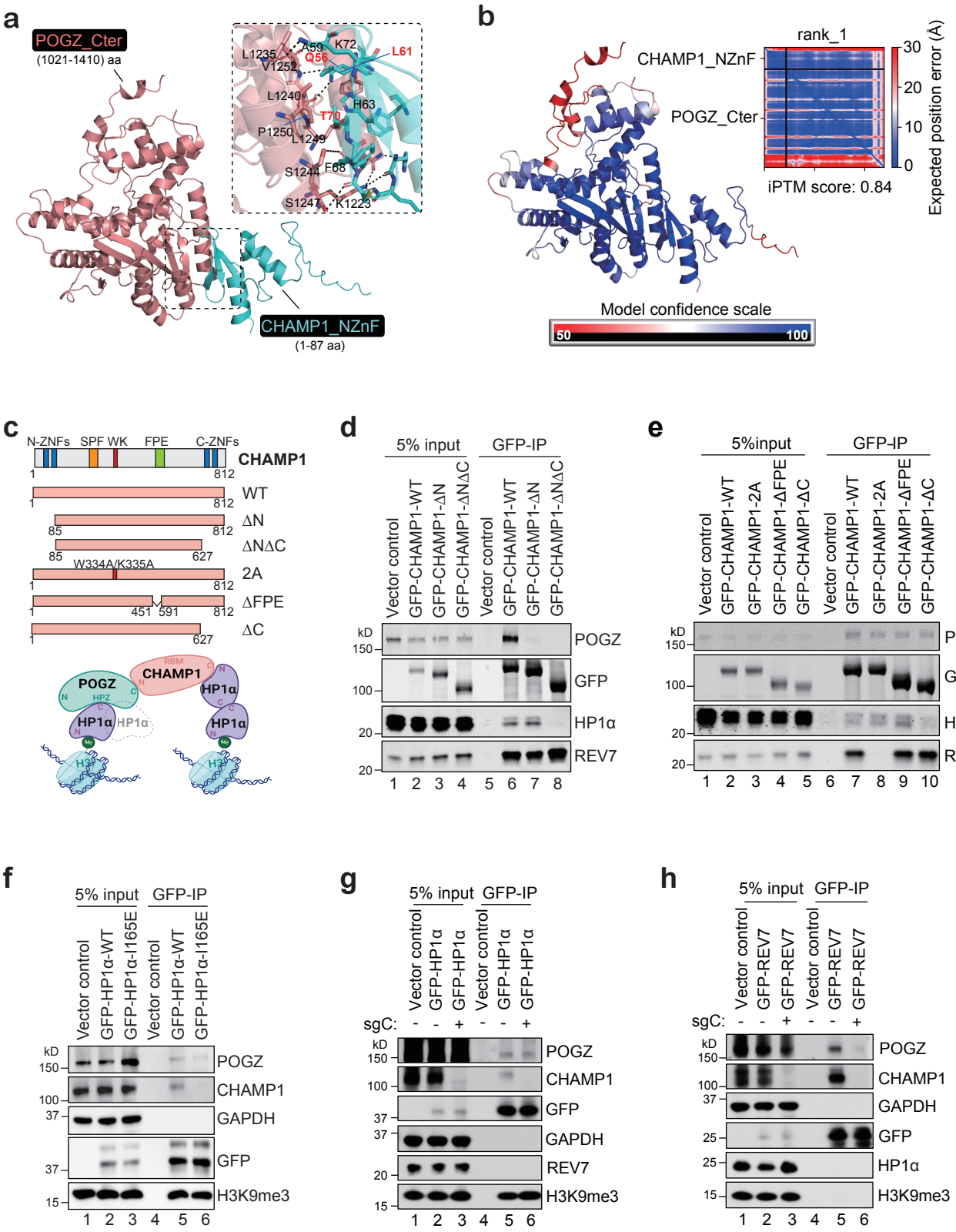
a
POGZ_Cter
(1021-1410) aa
CHAMP1_NZnF
(1-87 aa)
L1235
V1252
A59
Q56
K72
L61
L1240
H63
T70
P1250
L1249
S1244
F68
S1247
K1223
b
rank_1
CHAMP1_NZnF
POGZ_Cter
iPTM score: 0.84
Expected position error (Å)
Model confidence scale
50
100
c
N-ZNFs
SPF WK
FPE
C-ZNFs
CHAMP1
WT
ΔN
ΔNΔC
W334A/K335A
2A
ΔFPE
ΔC
POGZ
HP1α
d
5% input
GFP-IP
Vector control
GFP-CHAMP1-WT
GFP-CHAMP1-ΔN
GFP-CHAMP1-ΔNΔC
POGZ
GFP
HP1α
REV7
e
5%input
GFP-IP
GFP-CHAMP1-2A
GFP-CHAMP1-ΔFPE
GFP-CHAMP1-ΔC
f
GFP-HP1α-WT
GFP-HP1α-I165E
CHAMP1
GAPDH
H3K9me3
g
GFP-HP1α
sgC:
h
GFP-REV7

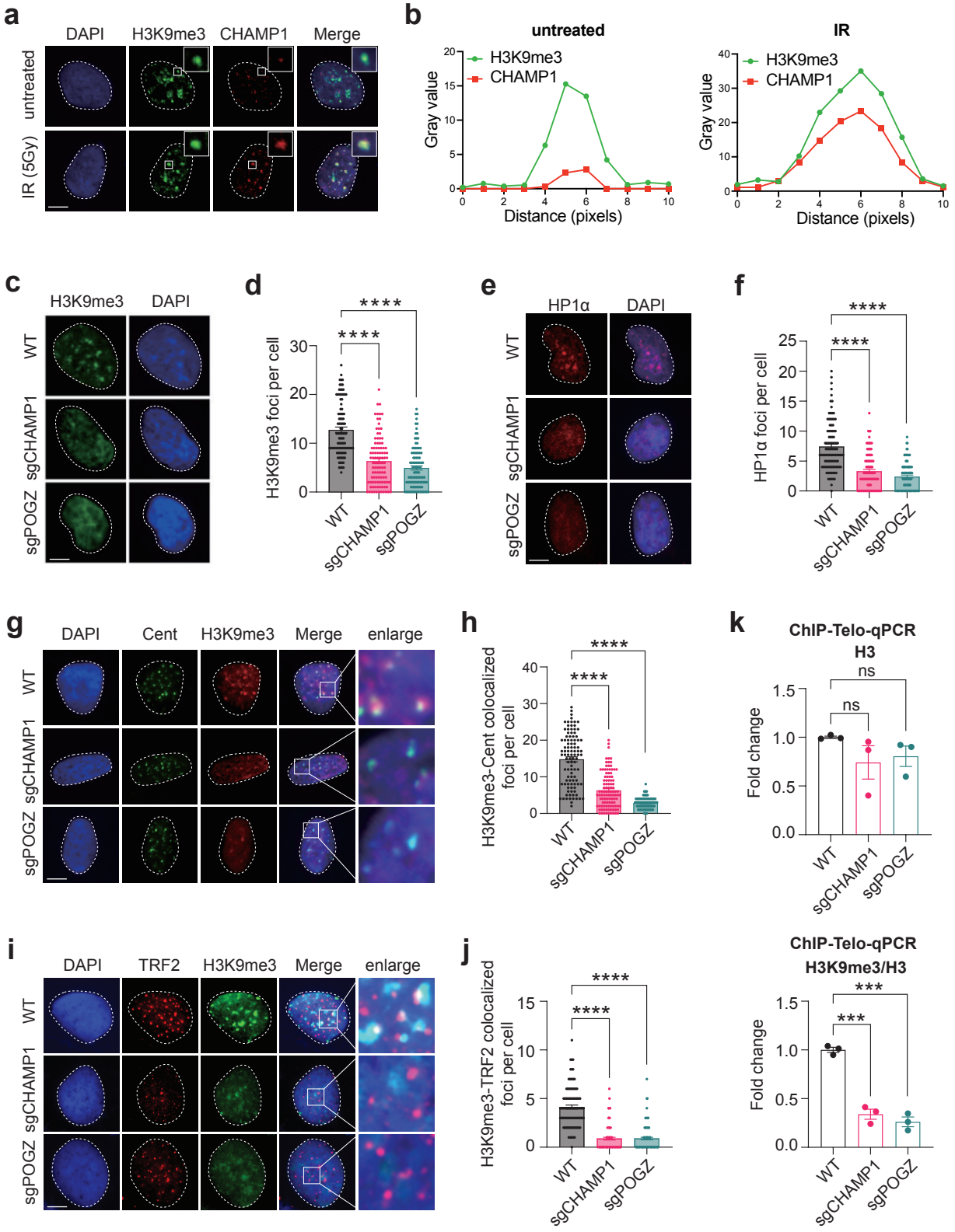
a
DAPI
H3K9me3
CHAMP1
Merge
untreated
IR (5Gy)
b
untreated
IR
H3K9me3
CHAMP1
Gray value
Distance (pixels)
c
H3K9me3
DAPI
WT
sgCHAMP1
sgPOGZ
d
H3K9me3 foci per cell
****
e
HP1α
DAPI
f
HP1α foci per cell
g
DAPI
Cent
H3K9me3
Merge
enlarge
h
H3K9me3-Cent colocalized foci per cell
k
ChIP-Telo-qPCR
H3
ns
Fold change
i
DAPI
TRF2
H3K9me3
Merge
enlarge
j
H3K9me3-TRF2 colocalized foci per cell
ChIP-Telo-qPCR
H3K9me3/H3
***

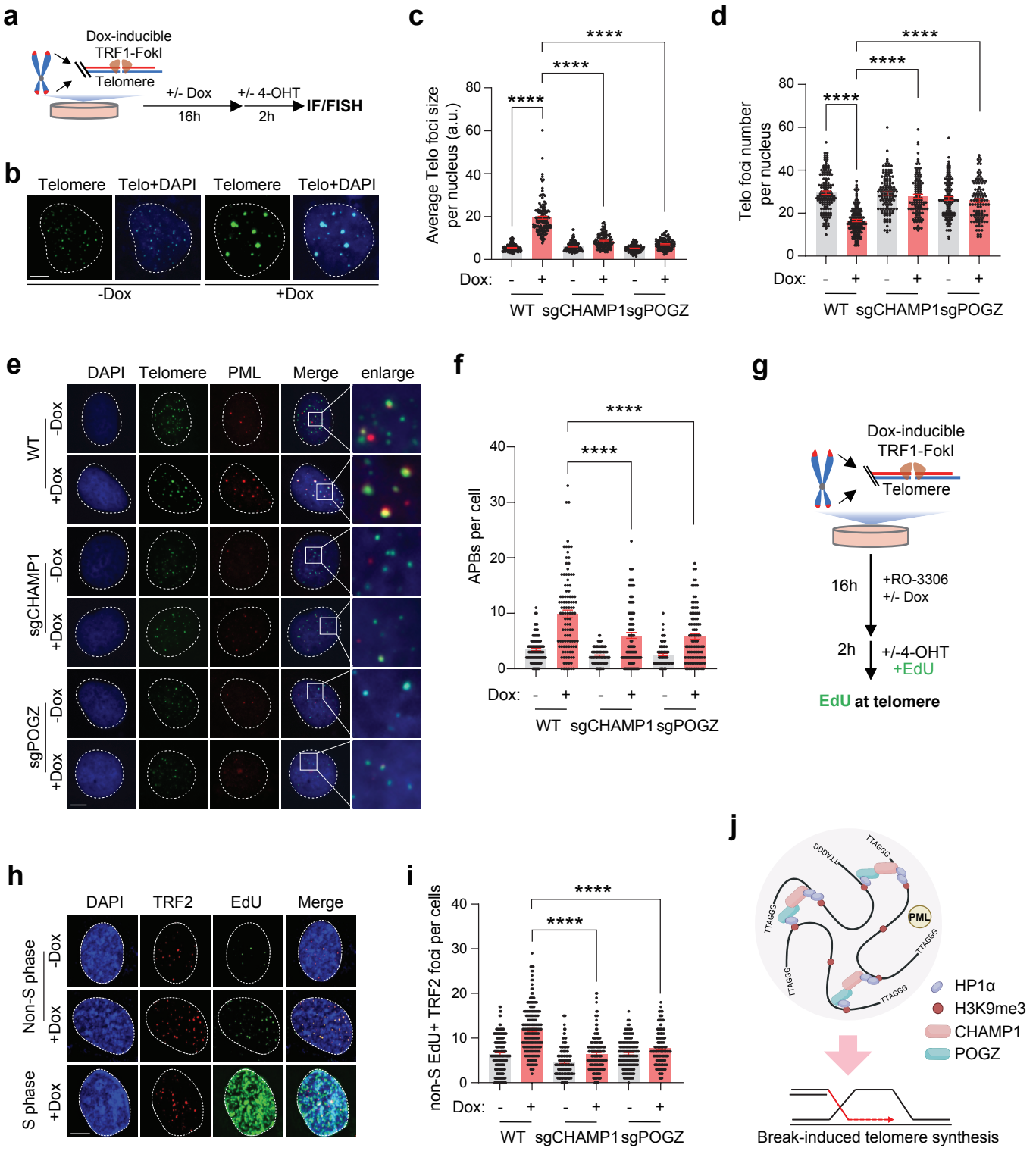
a
Dox-inducible
TRF1-FokI
Telomere
+/- Dox
16h
+/- 4-OHT
2h
IF/FISH
b
Telomere
Telo+DAPI
Telomere
Telo+DAPI
-Dox
+Dox
c
Average Telo foci size per nucleus (a.u.)
Dox:
WT
sgCHAMP1
sgPOGZ
d
Telo foci number per nucleus
e
DAPI
Telomere
PML
Merge
enlarge
WT
sgCHAMP1
sgPOGZ
-Dox
+Dox
f
APBs per cell
g
Dox-inducible
TRF1-FokI
Telomere
16h
+RO-3306
+/- Dox
2h
+/-4-OHT
+EdU
EdU at telomere
h
DAPI
TRF2
EdU
Merge
Non-S phase
S phase
i
non-S EdU+ TRF2 foci per cells
j
HP1α
H3K9me3
CHAMP1
POGZ
PML
Break-induced telomere synthesis

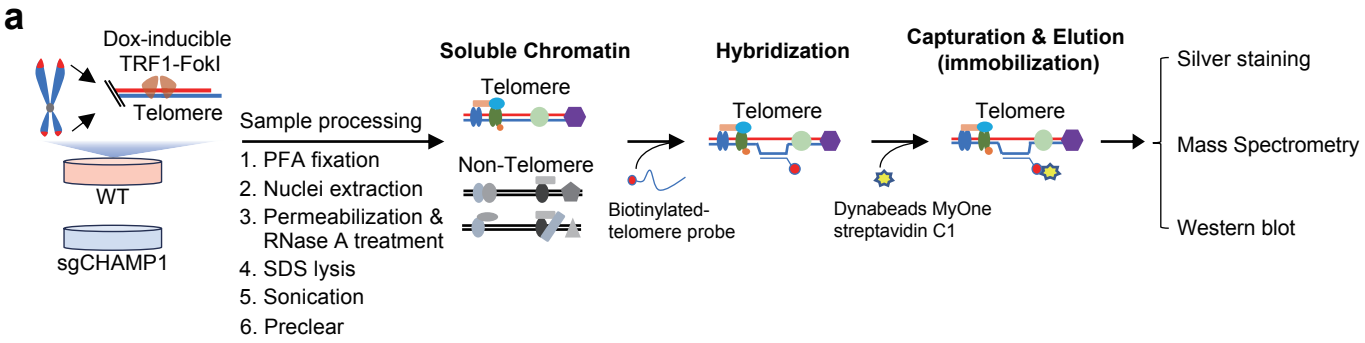
a
Dox-inducible TRF1-FokI
Telomere
WT
sgCHAMP1
Sample processing
1. PFA fixation
2. Nuclei extraction
3. Permeabilization & RNase A treatment
4. SDS lysis
5. Sonication
6. Preclear
Soluble Chromatin
Telomere
Non-Telomere
Biotinylated-telomere probe
Hybridization
Telomere
Dynabeads MyOne streptavidin C1
Capturation & Elution (immobilization)
Telomere
Silver staining
Mass Spectrometry
Western blot

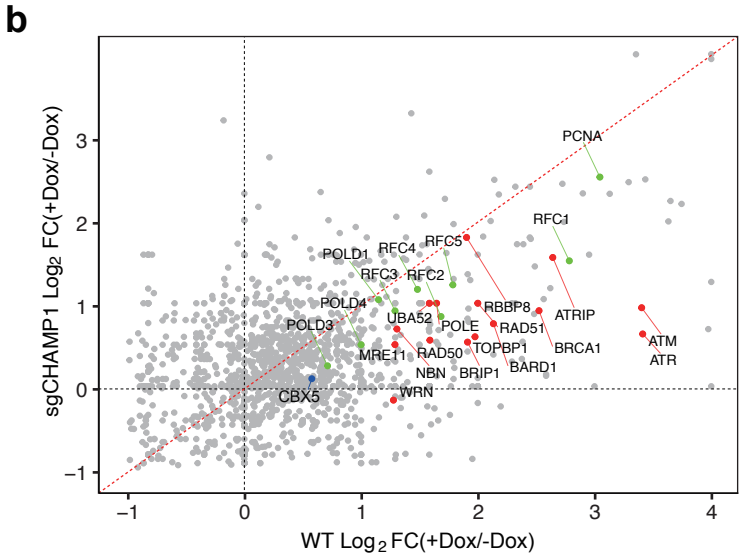
b
sgCHAMP1 Log2 FC(+Dox/-Dox)
WT Log2 FC(+Dox/-Dox)
PCNA
RFC1
POLD1
RFC4
RFC5
RFC3
RFC2
POLD4
POLD3
UBA52
RBBP8
POLE
RAD51
ATRIP
MRE11
RAD50
TOPBP1
BRCA1
ATM
ATR
NBN
BRIP1
BARD1
WRN
CBX5

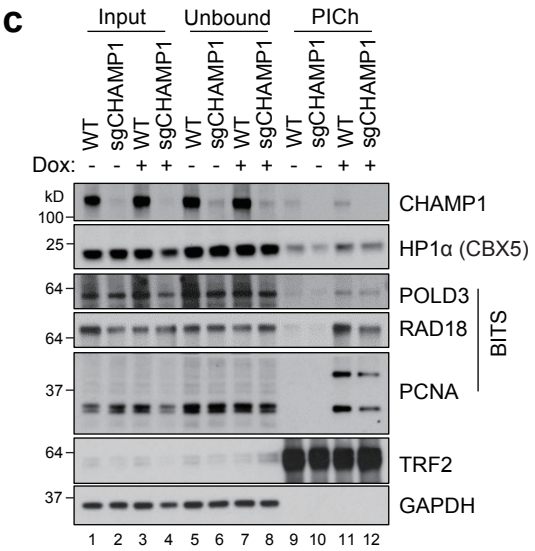
c
Input
Unbound
PICh
WT
sgCHAMP1
Dox:
kD
CHAMP1
HP1α (CBX5)
POLD3
RAD18
BITS
PCNA
TRF2
GAPDH
1 2 3 4 5 6 7 8 9 10 11 12

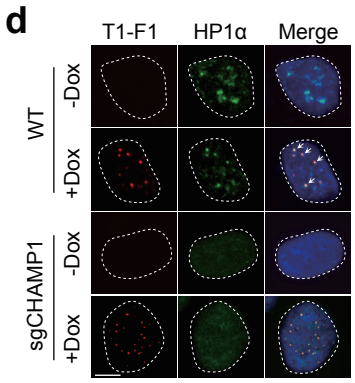
d
T1-F1
HP1α
Merge
WT
sgCHAMP1
-Dox
+Dox

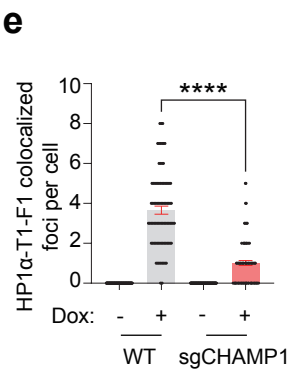
e
HP1α-T1-F1 colocalized foci per cell
****
Dox:
WT
sgCHAMP1

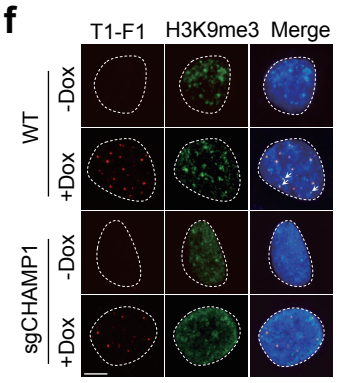
f
T1-F1
H3K9me3
Merge
WT
sgCHAMP1
-Dox
+Dox

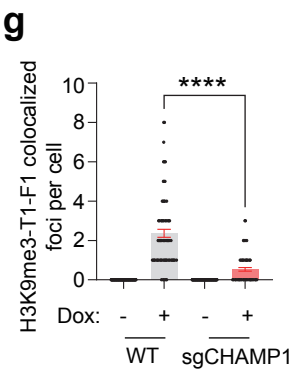
g
H3K9me3-T1-F1 colocalized foci per cell
****
Dox:
WT
sgCHAMP1

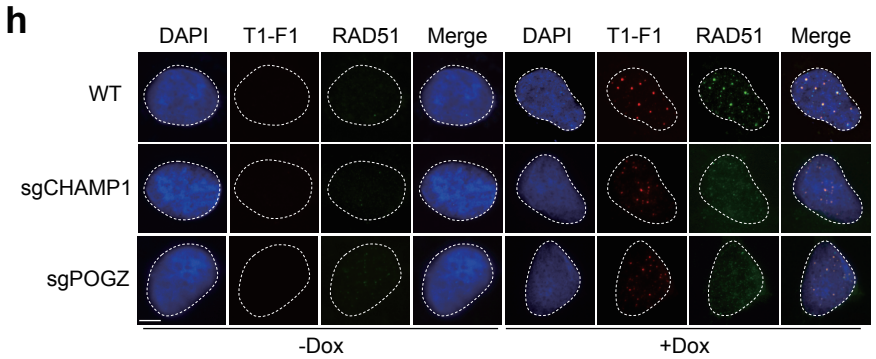
h
DAPI
T1-F1
RAD51
Merge
WT
sgCHAMP1
sgPOGZ
-Dox
+Dox

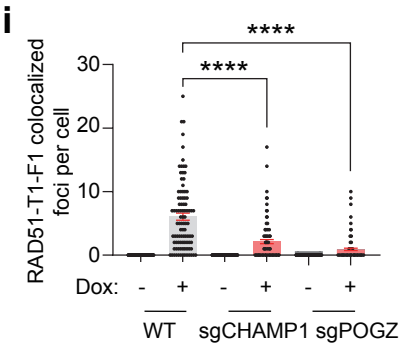
i
RAD51-T1-F1 colocalized foci per cell
****
****
Dox:
WT
sgCHAMP1
sgPOGZ

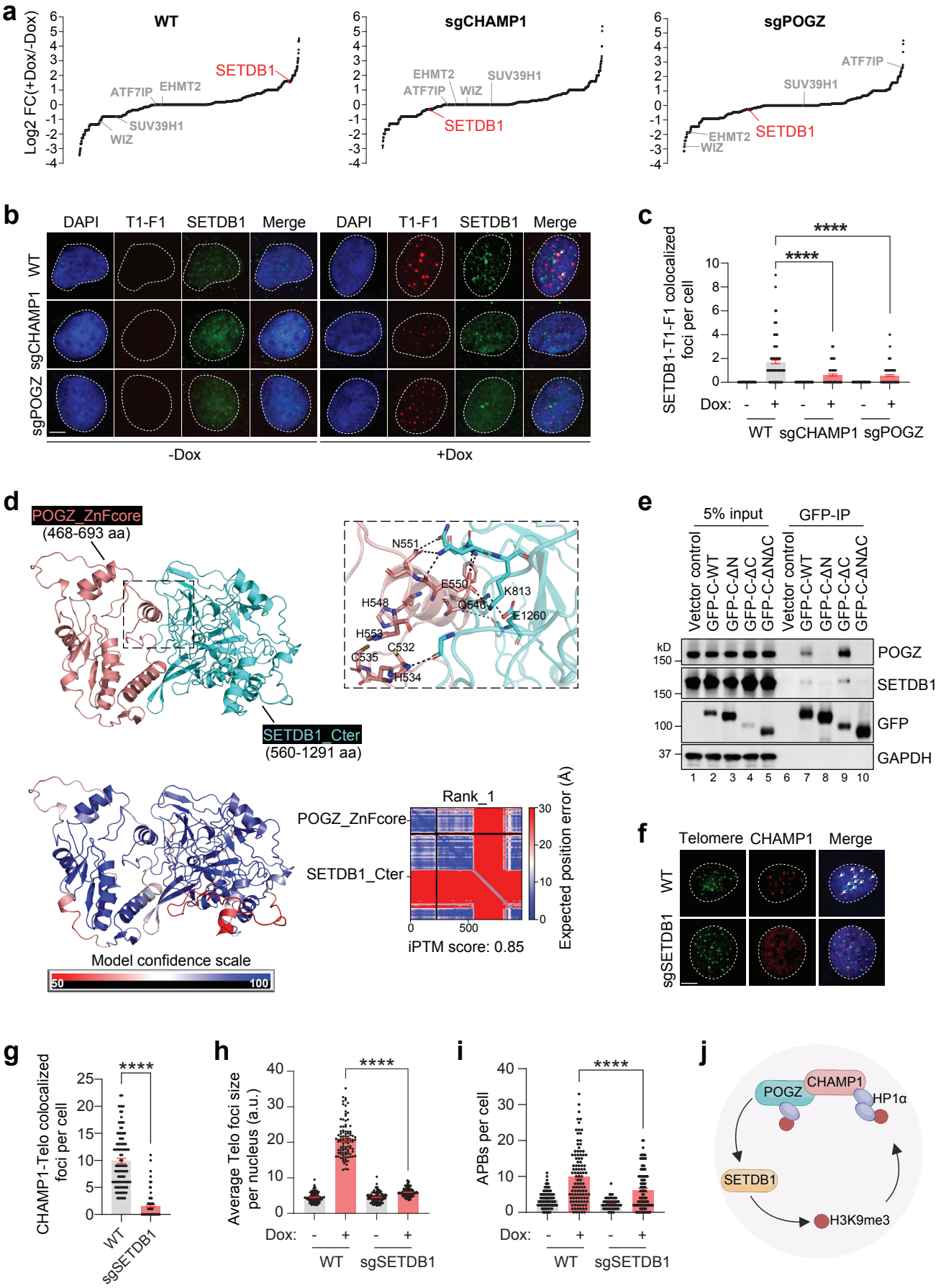
a
WT
sgCHAMP1
sgPOGZ
Log2 FC(+Dox/-Dox)
SETDB1
ATF7IP
EHMT2
SUV39H1
WIZ
b
DAPI
T1-F1
SETDB1
Merge
WT
sgCHAMP1
sgPOGZ
-Dox
+Dox
c
SETDB1-T1-F1 colocalized foci per cell
****
Dox:
WT
sgCHAMP1
sgPOGZ
d
POGZ_ZnFcore
(468-693 aa)
SETDB1_Cter
(560-1291 aa)
N551
E550
K813
H548
Q546
E1260
H553
C532
C535
H534
Rank_1
POGZ_ZnFcore
SETDB1_Cter
iPTM score: 0.85
Expected position error (Å)
Model confidence scale
50
100
e
5% input
GFP-IP
Vetctor control
GFP-C-WT
GFP-C-ΔN
GFP-C-ΔC
GFP-C-ΔNΔC
kD
POGZ
SETDB1
GFP
GAPDH
f
Telomere
CHAMP1
Merge
WT
sgSETDB1
g
CHAMP1-Telo colocalized foci per cell
****
WT
sgSETDB1
h
Average Telo foci size per nucleus (a.u.)
****
Dox:
WT
sgSETDB1
i
APBs per cell
****
Dox:
WT
sgSETDB1
j
POGZ
CHAMP1
HP1α
SETDB1
H3K9me3

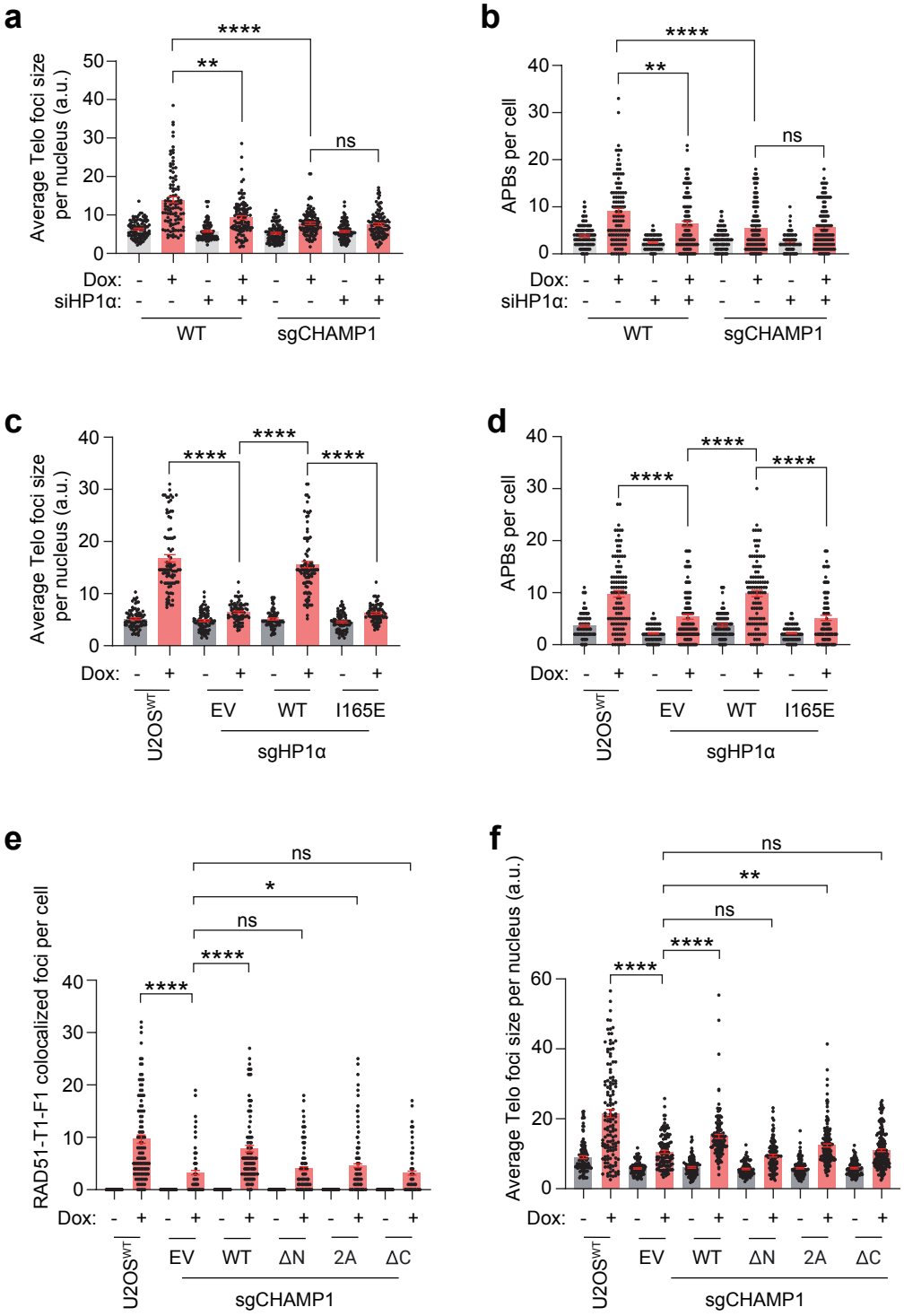
a
Average Telo foci size per nucleus (a.u.)
****
**
ns
Dox:
siHP1α:
WT
sgCHAMP1
b
APBs per cell
****
**
ns
Dox:
siHP1α:
WT
sgCHAMP1
c
Average Telo foci size per nucleus (a.u.)
****
****
****
Dox:
U2OS^WT
EV
WT
I165E
sgHP1α
d
APBs per cell
****
****
****
Dox:
U2OS^WT
EV
WT
I165E
sgHP1α
e
RAD51-T1-F1 colocalized foci per cell
ns
*
ns
****
****
Dox:
U2OS^WT
EV
WT
ΔN
2A
ΔC
sgCHAMP1
f
Average Telo foci size per nucleus (a.u.)
ns
**
ns
****
****
Dox:
U2OS^WT
EV
WT
ΔN
2A
ΔC
sgCHAMP1

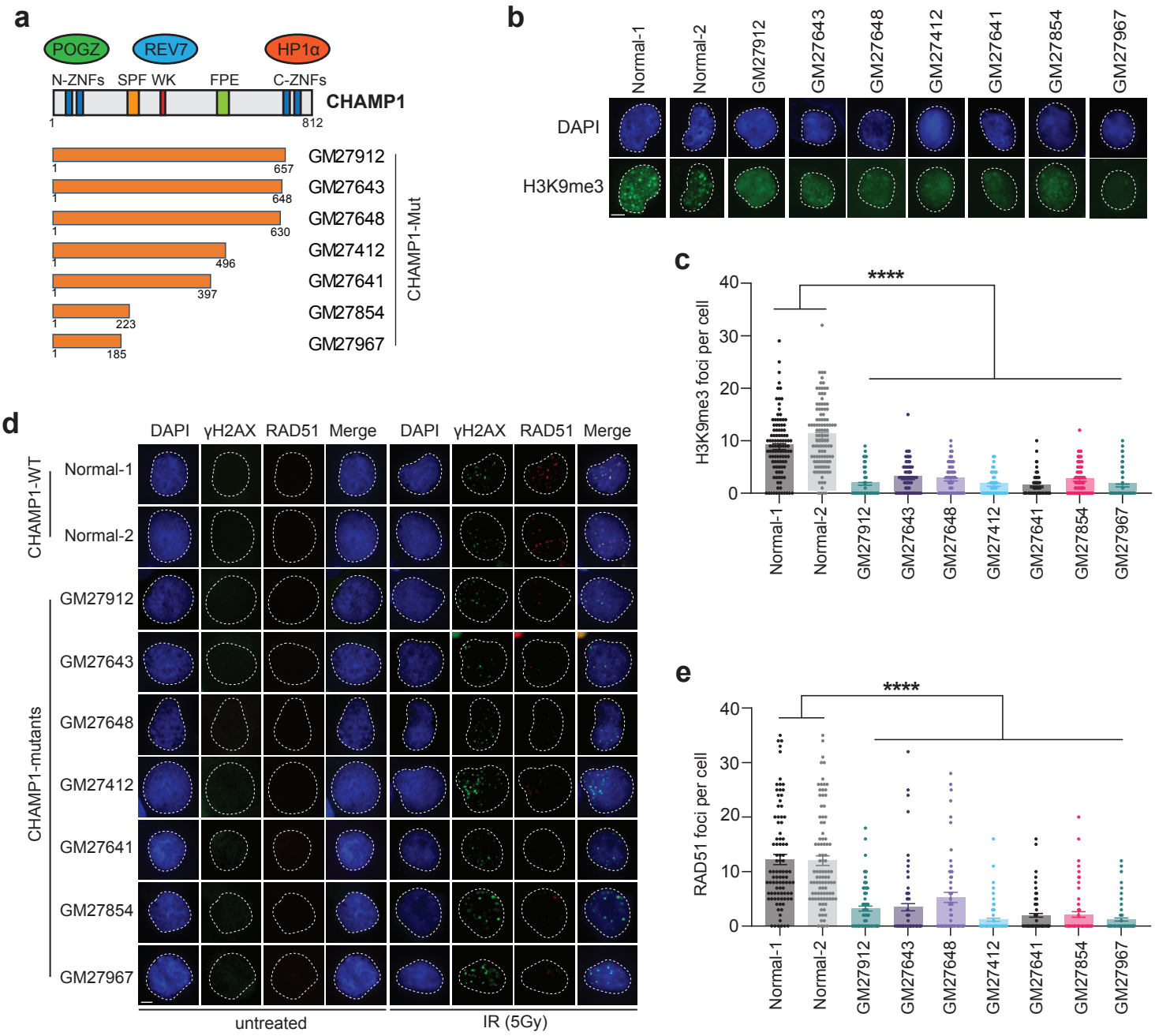
a
POGZ
REV7
HP1α
N-ZNFs
SPF WK
FPE
C-ZNFs
CHAMP1
1
812
GM27912
GM27643
GM27648
GM27412
GM27641
GM27854
GM27967
CHAMP1-Mut
657
648
630
496
397
223
185
b
Normal-1
Normal-2
GM27912
GM27643
GM27648
GM27412
GM27641
GM27854
GM27967
DAPI
H3K9me3
c
H3K9me3 foci per cell
****
d
DAPI
γH2AX
RAD51
Merge
CHAMP1-WT
CHAMP1-mutants
untreated
IR (5Gy)
e
RAD51 foci per cell
****

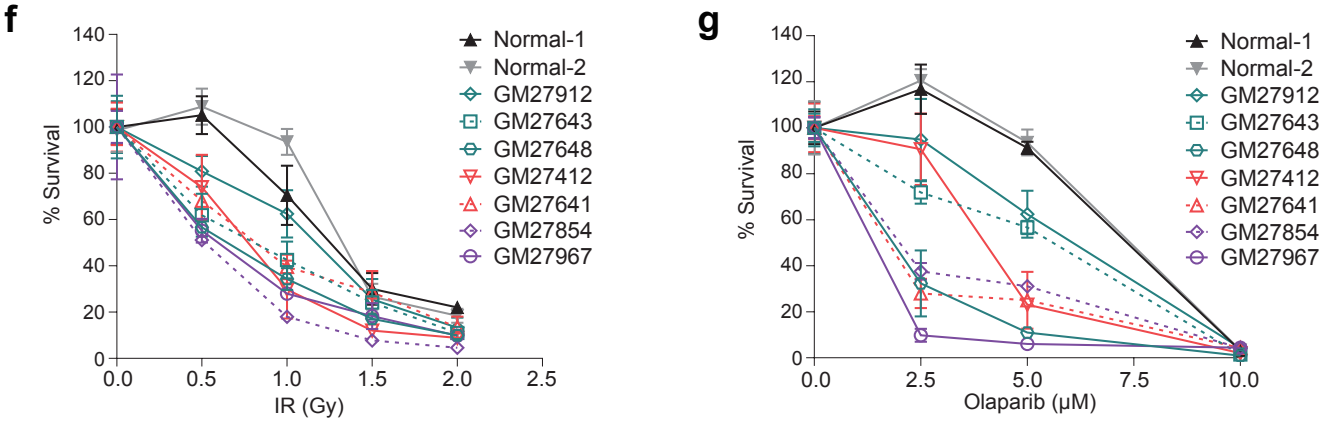
f
% Survival
IR (Gy)
Normal-1
Normal-2
GM27912
GM27643
GM27648
GM27412
GM27641
GM27854
GM27967
g
% Survival
Olaparib (μM)

Extended Data Fig. 1

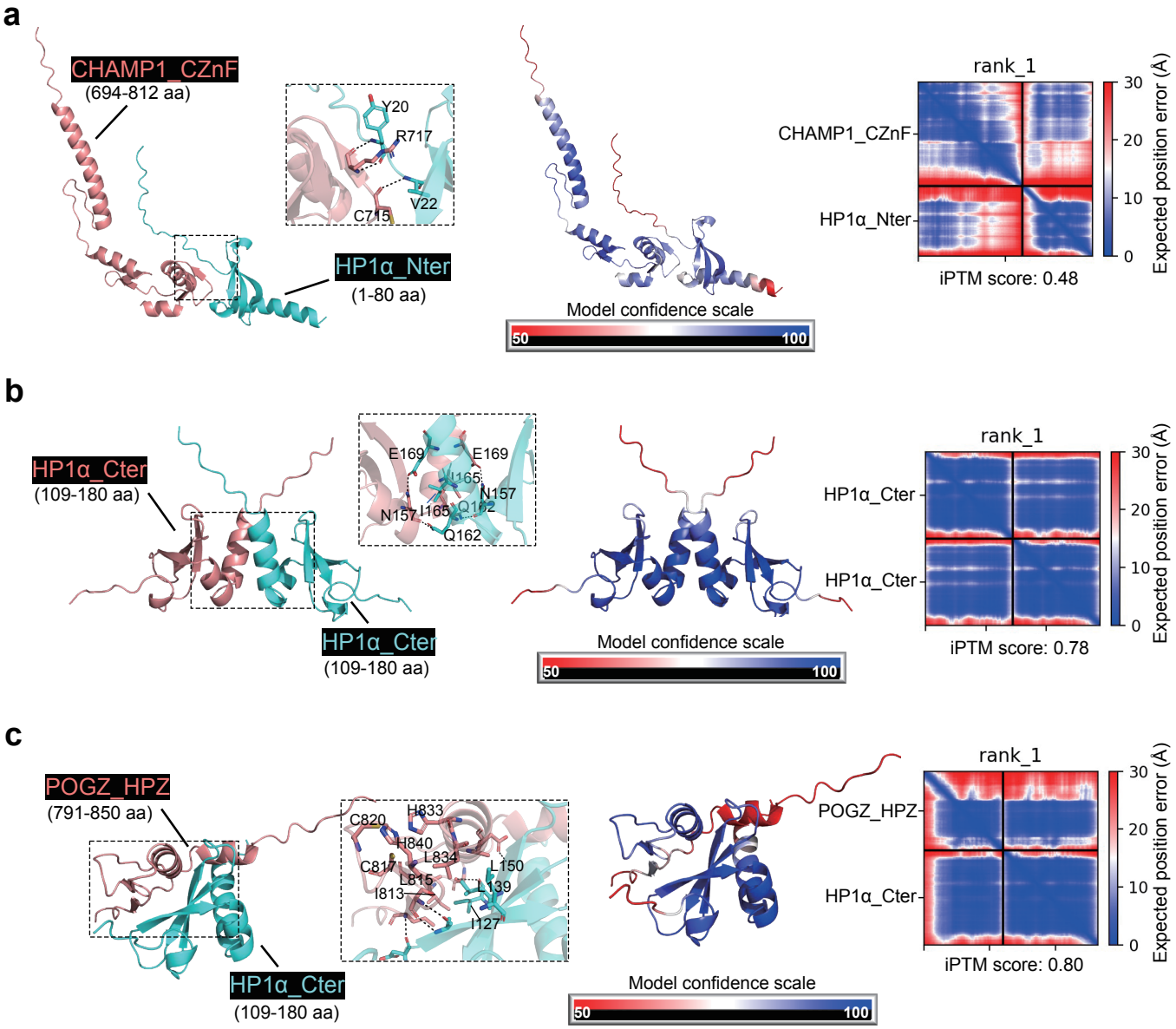

d

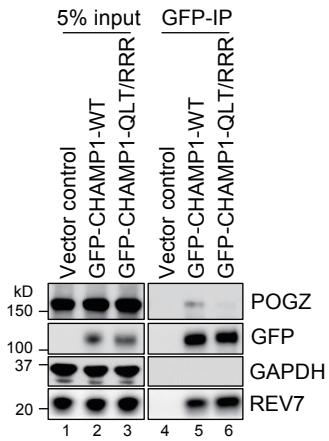

Extended Data Fig. 2

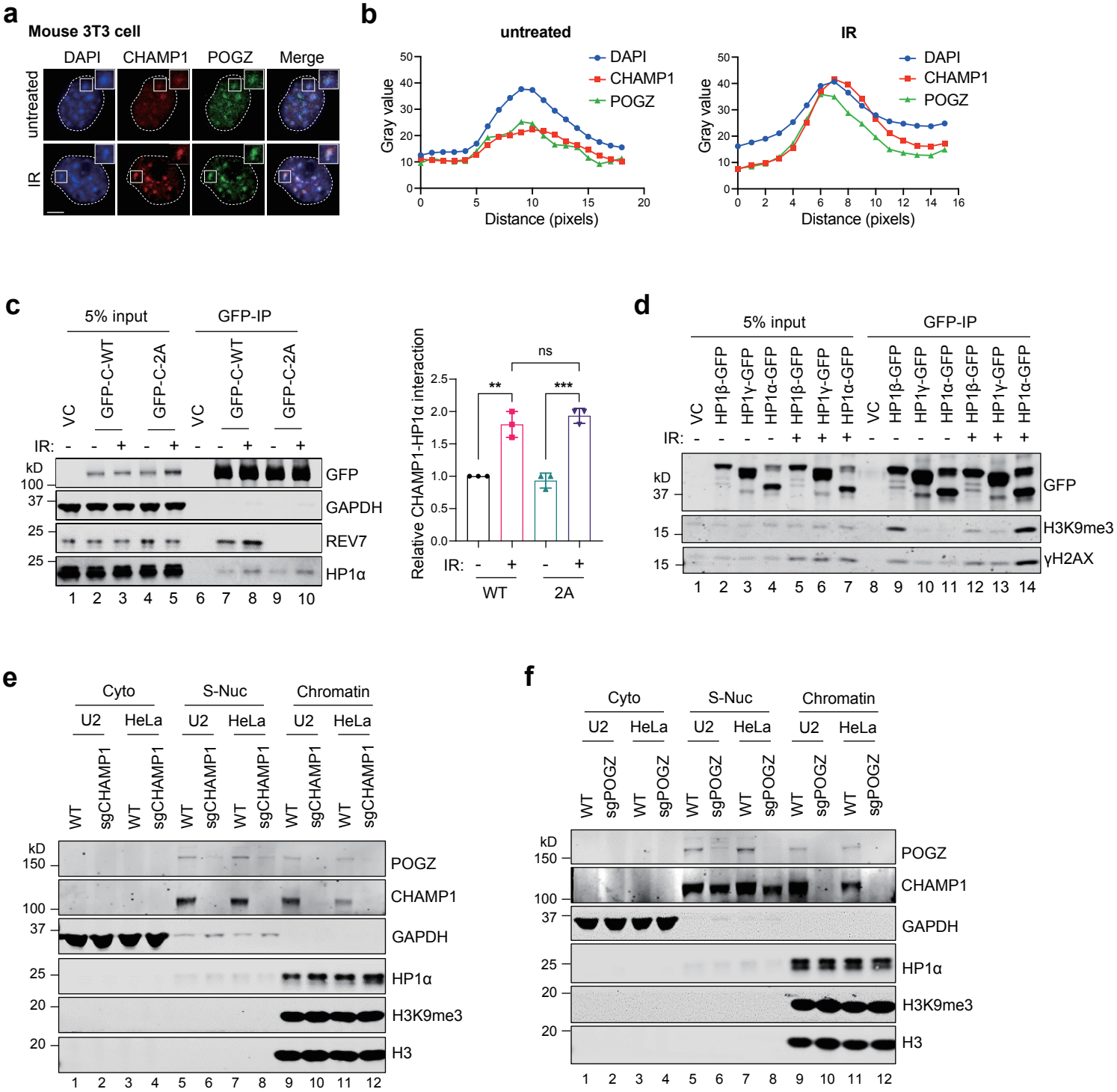

Extended Data Fig. 3

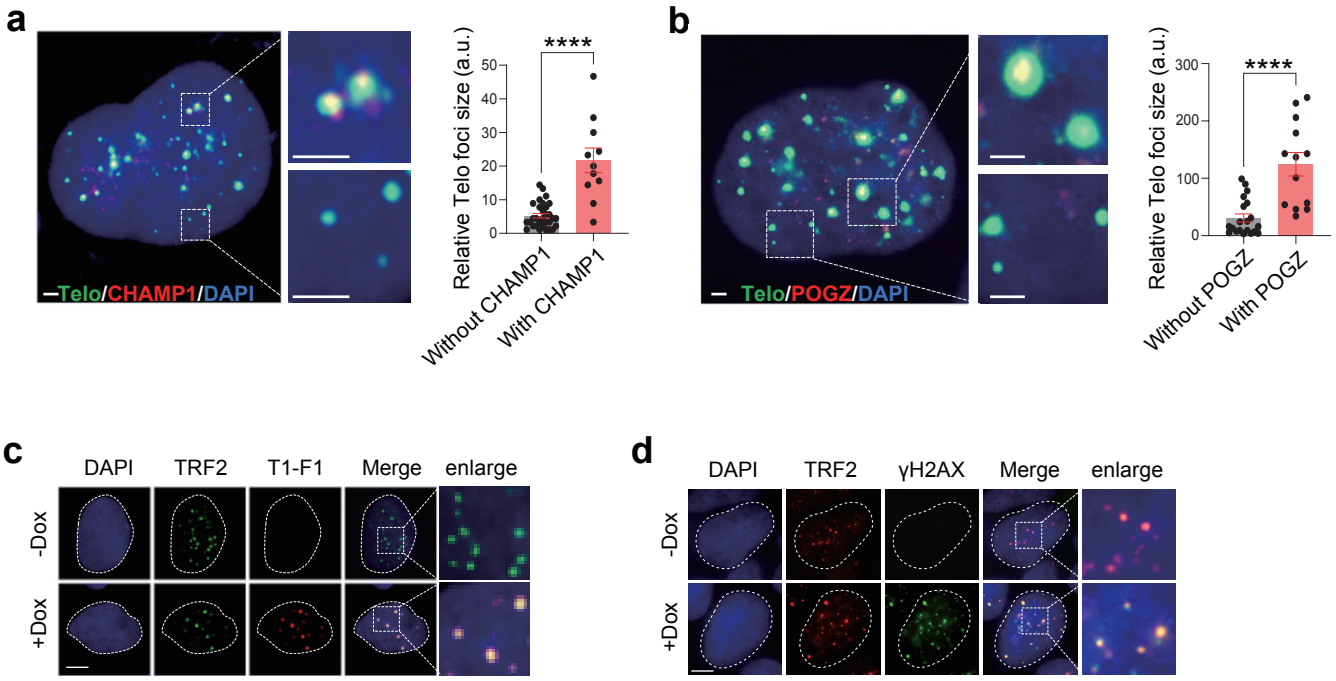

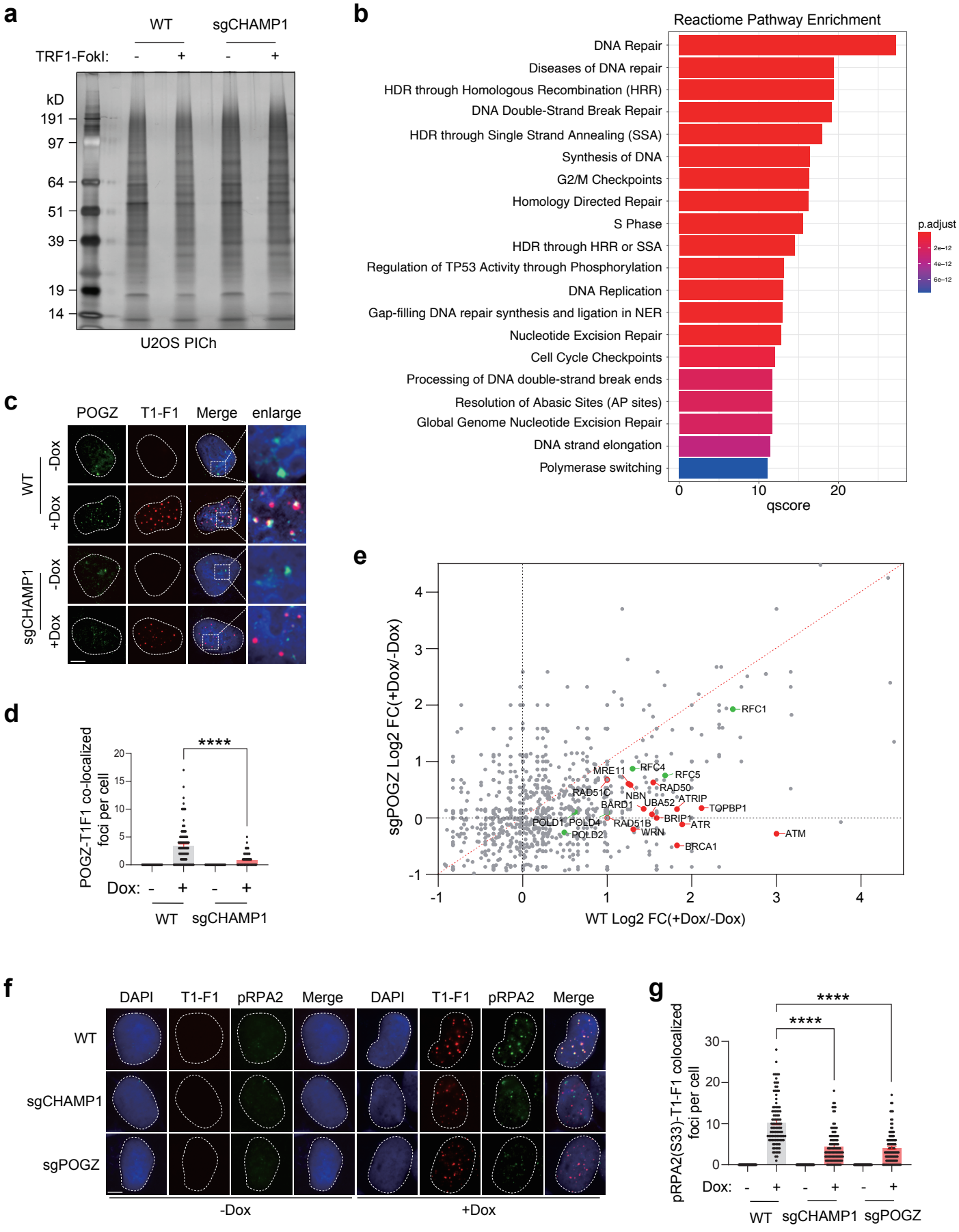
a
WT
sgCHAMP1
TRF1-FokI: - + - +
kD
191
97
64
51
39
19
14
U2OS PICh
b
Reactiome Pathway Enrichment
DNA Repair
Diseases of DNA repair
HDR through Homologous Recombination (HRR)
DNA Double-Strand Break Repair
HDR through Single Strand Annealing (SSA)
Synthesis of DNA
G2/M Checkpoints
Homology Directed Repair
S Phase
HDR through HRR or SSA
Regulation of TP53 Activity through Phosphorylation
DNA Replication
Gap-filling DNA repair synthesis and ligation in NER
Nucleotide Excision Repair
Cell Cycle Checkpoints
Processing of DNA double-strand break ends
Resolution of Abasic Sites (AP sites)
Global Genome Nucleotide Excision Repair
DNA strand elongation
Polymerase switching
0
10
20
qscore
p.adjust
2e−12
4e−12
6e−12
c
POGZ
T1-F1
Merge
enlarge
WT
-Dox
+Dox
sgCHAMP1
-Dox
+Dox
d
POGZ-T1F1 co-localized foci per cell
****
Dox: - + - +
WT
sgCHAMP1
e
sgPOGZ Log2 FC(+Dox/-Dox)
WT Log2 FC(+Dox/-Dox)
RFC1
MRE11
RFC4
RFC5
RAD50
RAD51C
NBN
ATRIP
BARD1
UBA52
TOPBP1
BRIP1
POLD1
POLD4
RAD51B
ATR
POLD2
WRN
ATM
BRCA1
f
DAPI
T1-F1
pRPA2
Merge
WT
sgCHAMP1
sgPOGZ
-Dox
+Dox
g
pRPA2(S33)-T1-F1 colocalized foci per cell
****
****
Dox: - + - + - +
WT
sgCHAMP1
sgPOGZ

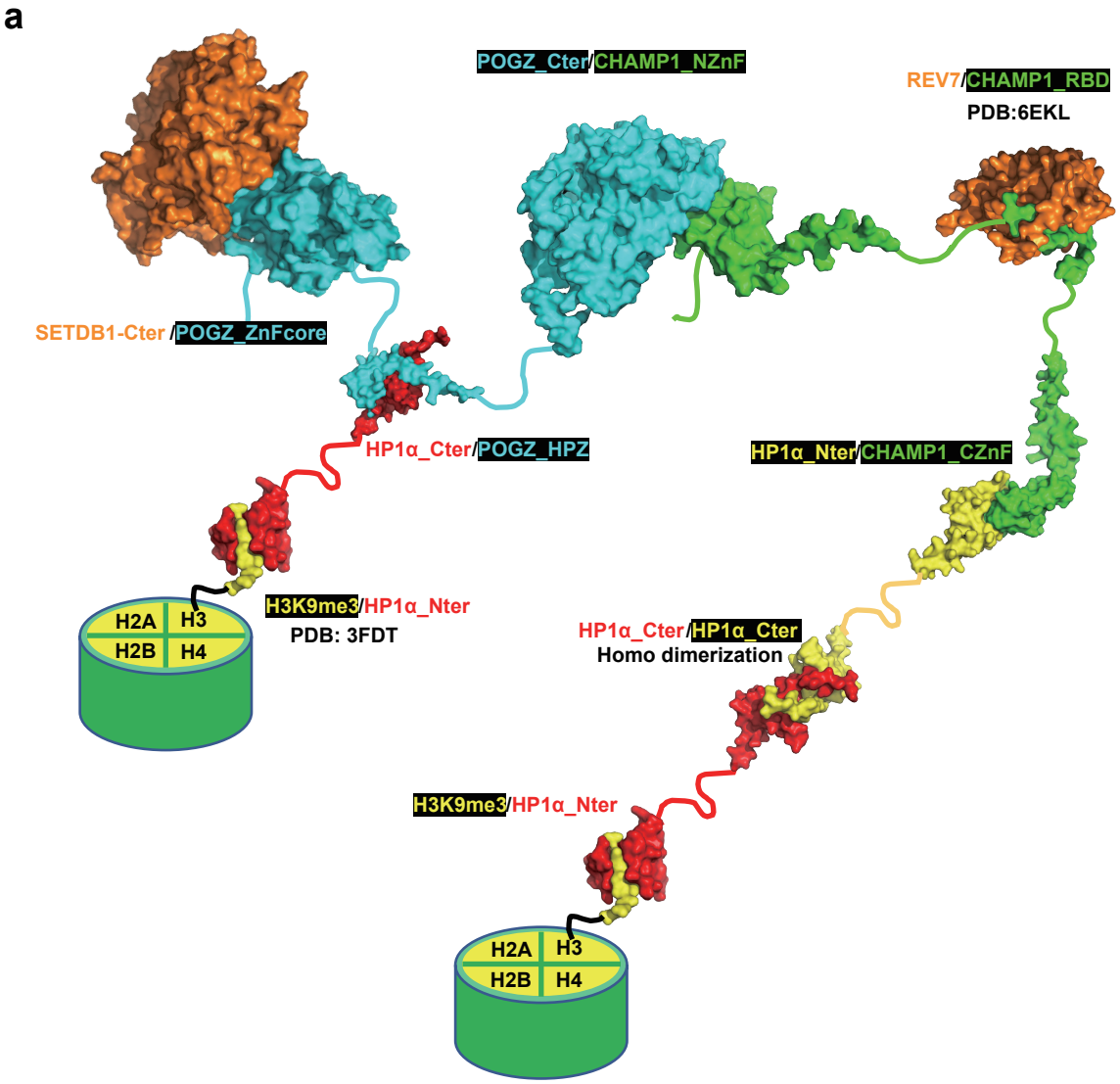
a
POGZ_Cter/CHAMP1_NZnF
REV7/CHAMP1_RBD
PDB:6EKL
SETDB1-Cter /POGZ_ZnFcore
HP1α_Cter/POGZ_HPZ
HP1α_Nter/CHAMP1_CZnF
H2A
H3
H2B
H4
H3K9me3/HP1α_Nter
PDB: 3FDT
HP1α_Cter/HP1α_Cter
Homo dimerization
H3K9me3/HP1α_Nter
H2A
H3
H2B
H4

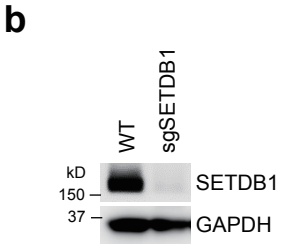
b
WT
sgSETDB1
kD
150
37
SETDB1
GAPDH

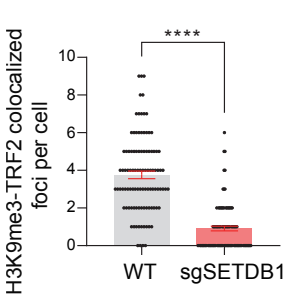
c
H3K9me3-TRF2 colocalized foci per cell
****
10
8
6
4
2
0
WT
sgSETDB1

Extended Data Fig. 6

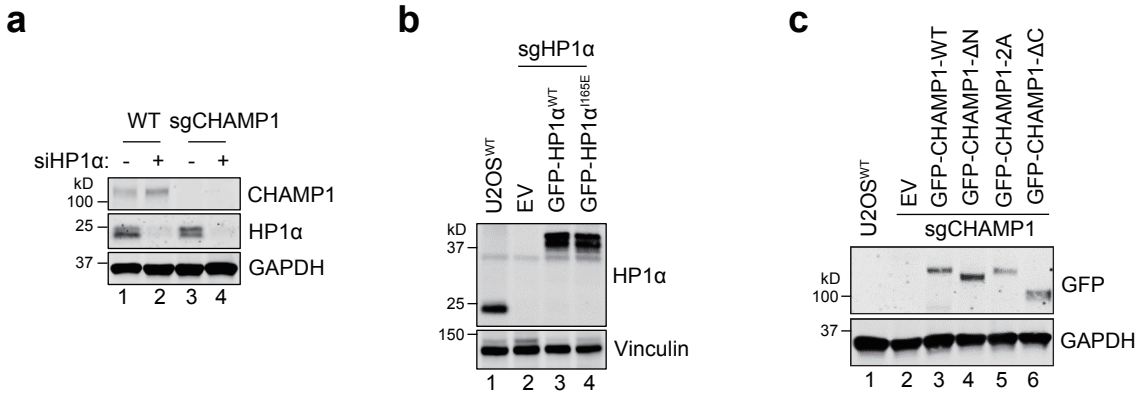

Extended Data Fig. 7

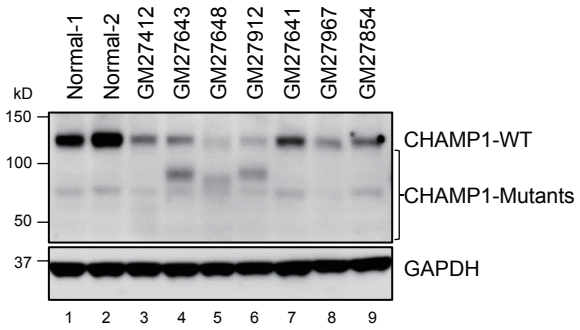

Extended Data Figure Legends

Extended Data Fig. 1, related to Fig. 1. CHAMP1, POGZ, and HP1α combine to create a complex. a. AF2-predicted structural model of CHAMP1_CZnF (peach)-HP1α_Nter (cyan). The key residues (shown in sticks) contributing to the formation of extended β-sheet interactions between CHAMP1 and HP1α are highlighted in the inset. The AF2-predicted model of CHAMP1_CZnF-HP1α_Nter complex is colored based on the confidence in the model prediction (100-high (blue) and 50-low (red)) and corresponding PAE matrix showing the confidence in the predicted interaction between CHAMP1_CZnF and HP1α_Nter along with iPTM score for the AF2 prediction. **b.** AlphaFold2-Multimer (AF2)-predicted structural model of homodimerization of HP1α_Cter. The key residues (shown in sticks) contributing to the protein-protein interactions are highlighted in the inset including HP1α residue (I165) that is shown to disrupt the homodimerization of HP1α when mutated. The AF2-predicted model of HP1α_Cter dimer is colored based on the confidence in the model prediction (100-high (blue) and 50-low (red)) and corresponding PAE matrix showing the confidence in the predicted interaction between two HP1α_Cter domains along with iPTM score for the AF2 prediction. **c.** AF2-predicted structural model of POGZ_HPZ (peach)-HP1α_Cter (cyan). The key residues (shown in sticks) contributing to the protein-protein interactions are highlighted in the inset including residues (C817, C820, H833 and H840) from POGZ_HPZ forming a C2H2-type Zn finger which was shown to be critical to maintain interactions with HP1α. The AF2-predicted model of POGZ_HPZ- HP1α_Cter complex is colored based on the confidence in the model prediction (100-high (blue) and 50-low (red)) and corresponding PAE matrix showing the confidence in the predicted interaction between POGZ_HPZ motif and HP1α_Cter domain along with iPTM score for the AF2 prediction. **d.** Western blot showing GFP-immunoprecipitation of GFP-empty vector, GFP-CHAMP1-wild-type (WT) and GFP-CHAMP1-QLT/RRR mutant in 293T cells, and the co-immunoprecipitation of endogenous POGZ and REV7. GAPDH acts as negative control for IP.

Extended Data Fig. 2, related to Fig. 2. IR induces CHAMP1-POGZ-HP1α complex formation. a. Representative immunofluorescence (IF) confocal images of the colocalized CHAMP1 and POGZ at DAPI dense heterochromatin clusters with/without IR (5Gy) treatment in mouse NIH-3T3 cells. DAPI was used to stain the nuclei. Scale bar, 5 µm. **b**. Square analysis of the intensity and colocalization of DAPI, CHAMP1 and POGZ foci in (a). **c.** (Left) Western blot showing GFP-immunoprecipitation of GFP-tagged CHAMP1-WT and -2A mutant in 293T cells after IR (5Gy) treatment, and the co-immunoprecipitation of endogenous REV7 and HP1α. (Right) The bands of HP1α after IP was calculated using ImageJ. Error bars indicate SEM. **P<0.01, ***P<0.001, ns, non-significant. Statistical analysis was performed using two-tailed Student's t test. **d**. Western blot showing GFP-immunoprecipitation of GFP-tagged HP1β, HP1γ, HP1α in 293T cells after IR (5Gy) treatment, and the co-immunoprecipitation of endogenous H3K9me3 and γH2AX. **e**. Western blot showing the cytoplasmic (Cyto), soluble nuclear (S-Nuc) and chromatin fraction in wild-type (WT) and sgCHAMP1 U2OS and HeLa cells. **f.** Western blot showing the cytoplasmic (Cyto), soluble nuclear (S-Nuc) and chromatin fraction in WT and sgPOGZ U2OS and HeLa cells. All of the immunoblots are representative of at least two independent experiments.

Extended Data Fig. 3, related to Fig. 3. CHAMP1 complex binds to the large ALT telomeres. a-b. IF-FISH confocal analysis of the colocalization of CHAMP1 (a) or POGZ (b) and telomere using a telomere (Telo) probe (green). DAPI was used to stain the nuclei. Scale bar, 2 µm. Telomere size was calculated using ImageJ. Error bars indicate SEM. ****P<0.0001. Statistical analysis was performed using two-tailed Student's t test. **c**. The mCherry-tagged TRF1-FokI colocalizes with the shelterin protein TRF2. Representative IF confocal images of telomeric binding protein TRF2 (green) and TRF1-FokI (T1-F1, mCherry, red) in the U2OS-TRF1-FokI cells with/without Dox/4-OHT treatment. DAPI was used to stain the nuclei. Scale bar, 5 µm. **d**. Representative IF confocal images of telomeric binding protein TRF2 (red) and γH2AX (green) in the U2OS-TRF1-FokI cells with/without Dox/4-OHT treatment. DAPI was used to stain the nuclei. Scale bar, 5 µm.

Extended Data Fig. 4, related to Fig. 4. CHAMP1 complex promotes DSB HR and BIR repair at telomeres. a. Silver staining of telomere chromatin bound fractions enriched by PICh with telomeric probe in wild-type (WT) and sgCHAMP1 U2OS cells induced with/without TRF1-FokI for 2 hrs. **b.** Pathway analysis of the telomere-specific DSB response proteome enriched by PICh in WT U2OS cells. Mass Spectrometry data was shown in Table S1. **c**. Representative IF confocal images showing the colocalization of POGZ (Green) with TRF1-FokI (mCherry, Red) in WT and sgCHAMP1 U2OS cells induced with TRF1-FokI for 2 h. DAPI was used to stain the nuclei. Scale bar, 5 µm. **d**. Quantification of (c) for number of POGZ-mCherry colocalization events. Error bars indicate SEM. More than 100 cells were counted. ****P<0.0001. Statistical analysis was performed using two-tailed Student's t test. **e.** Scatterplot of the telomere specific DSB response proteome profile enriched by PICh in wild-type (WT) and sgPOGZ U2OS cells induced with TRF1-FokI. Mass Spectrometry data was shown in Table S2. Scatterplot shows Log2 FC[(+Dox+1)/(-Dox+1) of total peptide number]. FC, fold change. Homologous recombination (HR) pathway proteins with Log2 FC > 0.5 in WT were highlighted in red. Break-induced replication (BIR) pathway proteins with Log2 FC > 0.5 in WT were highlighted in green. The red dotted line indicates the same value of log2 FC(+Dox/-Dox) in both WT and sgCHAMP1 cells. **f**. Representative IF images depicting the colocalization of pRPA2(S33) (Green) with TRF1-FokI (mCherry, Red) in WT, sgCHAMP1 and sgPOGZ U2OS cells induced with/without TRF1-FokI for 2 hours. DAPI was used to stain the nuclei. Scale bar, 5 µm. **g**. Quantification of pRPA2(S33)-mCherry colocalization events in (f). Error bars indicate SEM. More than 100 cells were counted. ****P<0.0001. Statistical analysis was performed using two-tailed Student's t test.

Extended Data Fig. 5, related to Fig. 5. CHAMP1 complex recruits SETDB1 to promote heterochromatin formation at telomeres. a. AlphaFold2-Multimer (AF2)-predicted structural model showing the interaction of SETDB1 and the CHAMP1 complex. **b.** Immunoblotting against SETDB1 in WT and sgSETDB1 U2OS cells. GAPDH was used as a loading control. **c**. Quantification of H3K9me3-TRF2 colocalization in WT and sgSETDB1 U2OS cells. Error bars indicate SEM. More than 100 cells were counted. ****P<0.0001. Statistical analysis was performed using two-tailed Student's t test.

Extended Data Fig. 6, related to Fig. 6. CHAMP1 complex subunit interaction is crucial for ALT activity. a. Immunoblotting against CHAMP1 and HP1α in WT and sgCHAMP1 U2OS cells after siRNA treatment against HP1α. GAPDH was used as a loading control. **b**. Immunoblotting against HP1α was performed in WT, sgHP1α, and sgHP1α U2OS cells with ectopically expressed HP1α WT or mutant I165E. Vinculin was used as a loading control. **c**. Immunoblotting against GFP in WT, sgCHAMP1, and sgCHAMP1 U2OS cells with ectopically expressed CHAMP1 WT or mutants (ΔN, 2A and ΔC). GAPDH was used as a loading control.

Extended Data Fig. 7, related to Fig. 7. Lymphocyte cells from CHMAP1 patients express truncated CHAMP1 proteins. Western blot of CHAMP1 in EBV-immortalized lymphoblast cell lines derived from several CHAMP1 patients (Coriell). GAPDH acts as loading control.